Inorganic Chemistry

pubs.acs.org/IC
Article

Phenylbenzothiazole-Based Platinum(II) and Diplatinum(II) and (III) Complexes with Pyrazolate Groups: Optical Properties and Photocatalysis

David Gómez de Segura, Andrea Corral-Zorzano, Eduardo Alcolea, M. Teresa Moreno,* and Elena Lalinde*

Cite This: *Inorg. Chem.* 2024, 63, 1589−1606
Read Online

ACCESS | Metrics & More | Article Recommendations | Supporting Information

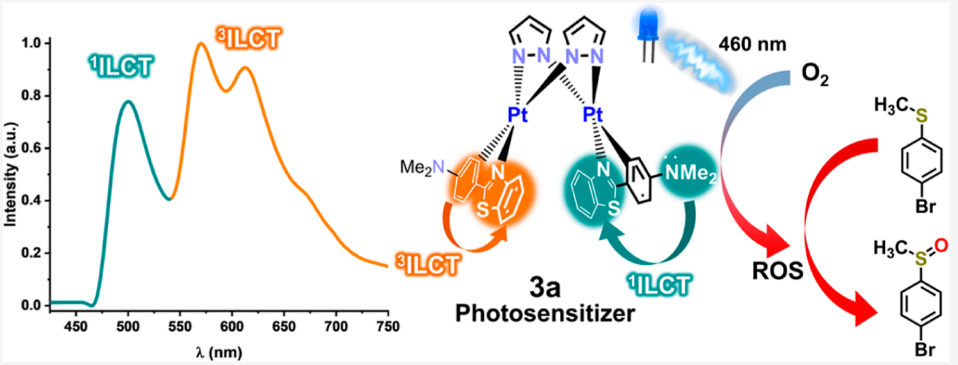

ABSTRACT: Based on 2-phenylbenzothiazole (pbt) and 2-(4-dimethylaminophenyl)benzothiazole (Me_2N-pbt), mononuclear $[Pt(pbt)(R'_2\text{-}pzH)_2]PF_6$ (R'_2-pzH = pzH **1a**, 3,5-Me_2pzH **1b**, 3,5-$^iPr_2$pzH **1c**) and diplatinum ($Pt^{II}-Pt^{II}$) $[Pt(pbt)(\mu\text{-}R'_2pz)]_2$ (R'_2-pz = pz **2a**, 3,5-Me_2pz **2b**, 3,5-$^iPr_2$pz **2c**) and $[Pt(Me_2N\text{-}pbt)(\mu\text{-}pz)]_2$ (**3a**) complexes have been prepared. In the presence of sunlight, **2a** and **3a** evolve, in $CHCl_3$ solution, to form the $Pt^{III}-Pt^{III}$ complexes $[Pt(R\text{-}pbt)(\mu\text{-}pz)Cl]_2$ (R = H **4a**, NMe_2 **5a**). Experimental and computational studies reveal the negligible influence of the pyrazole or pyrazolate ligands on the optical properties of **1a**−**c** and **2a**,**b**, which exhibit a typical ^{3}IL/^{3}MLCT emission, whereas in **2c** the emission has some ^{3}MMLCT contribution. **3a** displays unusual dual, fluorescence (^{1}ILCT or ^{1}MLCT/^{1}LC), and phosphorescence (^{3}ILCT) emissions depending on the excitation wavelength. The phosphorescence is lost in aerated solutions due to sensitization of $^3O_2$ and formation of $^1O_2$, whose determined quantum yield is also wavelength dependent. The phosphorescence can be reversibly photoinduced (365 nm, ∼ 15 min) in oxygenated THF and DMSO solutions. In **4a** and **5a**, the lowest electronic transitions (S_1-S_3) have mixed characters (LMMCT/LXCT/L'XCT **4a** and LMMCT/LXCT/ILCT **5a**) and they are weakly emissive in rigid media. The $^1O_2$ generation property of complex **3a** is successfully used for the photooxidation of *p*-bromothioanisol showing its potential application toward photocatalysis.

INTRODUCTION

Luminescent transition-metal compounds have attracted considerable attention owing to their wide range of applicability, such as emitters for light-emitting devices, optoelectronic materials, bioimagen probes, sensors, and photocatalysis.[1] Among these complexes, cyclometalated platinum complexes are considered one of the most promising materials due to their rich and tunable excited-state properties, which can be fine-tuned by molecular design.[2] Thus, mononuclear Pt^{II} complexes exhibit highly efficient triplet-state phosphorescence attributed to ^{3}LC($^3\pi\pi$), ^{3}MLCT, or ^{3}LC/^{3}MLCT and ^{3}LLCT/^{3}MLCT mixtures, depending on the cyclometalating and ancillary ligands. A remarkable feature of these complexes is their propensity to develop, in the ground and/or upon excitation, noncovalent *intermolecular* platinum−platinum contacts through the interaction of the filled $5d_{z^2}$ orbitals and $\pi\pi$ stacking interactions, particularly favored by the coordination of planar chelating aromatic ligands. These interactions are accompanied by simultaneous changes in the spectroscopic and optical properties, such as assembly-induced metal−metal−to ligand charge-transfer (MMLCT) transitions, which appear at lower energies than the corresponding monomers, and may be utilized to achieve single-doped white OLEDs[3] or stimuli-responsive functional materials.[4] Many of these systems have demonstrated

Received: October 9, 2023
Revised: November 21, 2023
Accepted: December 22, 2023
Published: January 10, 2024

https://doi.org/10.1021/acs.inorgchem.3c03532
Inorg. Chem. 2024, 63, 1589−1606

to be solid-state low-red or near-infrared (NIR) emitters, with attractive applications in OLEDs[5] or biological imaging.[6]

Another successful approach to modulate the optical properties is through the design of new bimetallic platinum(II) complexes in which the *intramolecular* Pt···Pt distance can be synthetically manipulated, primarily by the nature and bulkiness of the bridging ligands and to a minor extent by the cyclometalating groups. In addition, in bimetallic complexes, the efficiency is usually notably increased, which has been attributed to the enhanced coupling between the T_1 state and higher lying singlet states due to the incorporation of a second Pt center.[7] Considerable interest has focused on two main categories, one featuring a *butterfly* shape and pyrazolate bridging ligands with relatively longer metal−metal separations and the other having a *half-lantern* shape and bridging thiolates with shorter intermetallic distances (Chart 1). Indeed, very

Chart 1. Schematic Drawings of Diplatinum(II) and (III) Complexes Bearing Pyrazolate and N^S Bridging Ligands.

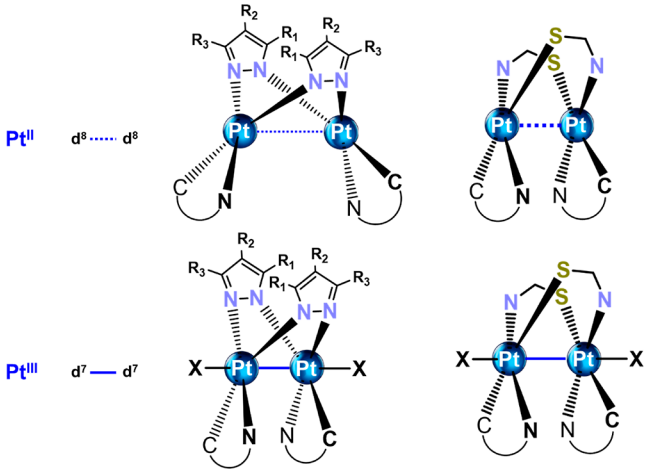

efficient NIR phosphorescent OLED emitters have been reported using single-emissive binuclear *half-lantern* cyclometalated complexes with various thiolates (pyridyl-thiolate, oxadiazole-thiolate, or benzo[*d*]thiazole-2-thiolate) as bridging ligands associated with a very strong ^{3}MMLCT emission due to relatively short Pt···Pt distances.[5b,8] In the *butterfly* shape, Pt^{II} complexes bearing pyrazolate bridging groups, the electronic structure mainly depends on the steric bulkiness of the substituent groups of the pyrazolate ligands, which modulates the Pt···Pt separation not only in the ground state but also in the excited state. When the Pt···Pt separation is relatively large, the low-lying transitions are due to mixed LC/MLCT excitations located on separated platinum units because, upon excitation, there is a local T_1 minimum with a similar geometry to the S_0 ground state. However, if the Pt···Pt separation are shorter, upon excitation, easy intersystem crossing (on a subpicosecond time scale) to the ^{1,3}MMCT state takes place, leading to a T_1-global minimum in which further contraction of Pt−Pt distance (∼0.2−0.3 Å) occurs, due to depopulation of the dσ*, characteristic of the ^{3}MMLCT excited state.[9] In these systems, the photoinduced molecular structural change that takes place upon excitation, strongly depends on the surrounding environment of the molecule and, as a consequence, access to both excited states occurs giving rise to dual emissions depending on the media and the concentration.[8a,10] The dynamics and properties of the excited states of these binuclear complexes have been explored by ultrafast spectroscopic techniques (femtosecond absorption spectroscopy) and density functional theory (DFT) calculations in recent years.[9a,11] The electronic characteristics of the chromophoric cyclometalating group also play a key role on the final electronic nature of these diplatinum complexes, but its effect has been comparatively less explored.[12] In this field, despite the tremendous role that Pt···Pt *nonbonded* interactions play on the optical properties of cycloplatinated complexes, much less attention has been devoted to complexes featuring formal covalent Pt−Pt bonds (Chart 1).[13] Indeed, in diplatinum cycloplatinated compounds, reports on emissive Pt^{III}−Pt^{III} (d^7−d^7) derivatives are quite rare.[14] In these complexes, the lowest lying excited state has usually a remarkable metal center character (dσ_M−dσ^*_M), being therefore nonemissive.

Heterocycles featuring benzothiazole frameworks have been widely recognized as biologically active compounds[15] and are also important fluorophores used to construct donor/acceptor systems displaying intramolecular charge-transfer properties.[16] In this context, over the past few years, we have focused on the design and study of the optical and biological properties of cyclometalated Pt^{II}, Pt^{IV}, and Ir^{III} mononuclear complexes based on 2-phenylbenzothiazole (pbt) and 2-(4-dimethylaminophenyl)benzothiazole (Me_2N-pbt) frameworks.[17] Following our interest in these systems, here we report new families of mononuclear [Pt(pbt)(R′$_2$-pzH)$_2$]PF$_6$ (R′$_2$-pzH = pzH **1a**, 3,5-Me_2pzH **1b**, 3,5-^{i}Pr$_2$pzH **1c**) and binuclear (Pt^{II}−Pt^{II}) [Pt(pbt)(μ-R′$_2$pz)]$_2$ (**2a−c**), [Pt(Me_2N-pbt)(μ-pz)]$_2$ (**3a**) and Pt^{III}−Pt^{III} [Pt(R-pbt)(μ-pz)Cl]$_2$ (R = H **4a**, NMe_2 **5a**) complexes based on phenylbenzothiazole (pbt) and 2-(4-dimethylaminophenyl)benzothiazole (Me_2N-pbt) as cyclometalated groups and different pyrazole (**1**) or pyrazolate (**2−5**) as bridging ligands. Their photophysical properties, supported by theoretical calculations, are presented.

On the other hand, sulfoxides, in particular asymmetric sulfoxides, are nowadays widely used in organic synthesis, fine chemicals, medicine, pesticides,[18] and, recently, have also emerged as efficient ligands in transition-metal catalysis.[19] Common oxidants for sulfide oxidation to sulfoxides (H_2O_2, $K_2S_2O_8$, or *m*-chloroperbenzoic acid) are usually not eco-friendly or cause serious environmental pollution. In recent years, photocatalytic oxidations have been successfully reported employing O_2 as an environmentally friendly oxidant and different organic photosensitizers, such as Rose Bengal,[20] Rivoflavin,[21] or Bodipy.[22] In this area, the employment of metal phosphorescent complexes as photosensitizers is rather less developed; although recently, the efficiency of several Ir^{III}, Ru^{II} and Au^{I} systems have been demonstrated.[23] To increase the knowledge on these systems, we sought to explore the utility of complex **3a**, which displayed strong oxygen sensitivity on its phosphorescent band, for the photocatalytic oxidation of sulfides using O_2 as a green oxidant.

RESULTS AND DISCUSSION

Synthesis and Characterization. *Synthesis and Characterization of Cationic Bis-Pyrazole Pt^{II} Complexes.* The reaction of the DMSO solvate [Pt(pbt)Cl(DMSO)][17e] with 1 equiv of TlPF$_6$ and 2 equiv of the corresponding pyrazole ligand in acetone at room temperature gives rise to new bis-pyrazole complexes of the type [Pt(pbt)(R′$_2$-pzH)$_2$]PF$_6$ (**1** R′$_2$-pzH = pzH (**a**), 3,5-Me_2pzH (**b**), and 3,5-^{i}Pr$_2$pzH (**c**)) (see Scheme 1 and Experimental Section). All attempts to generate related mononuclear complexes with the 2-(4-dimethylaminophenyl)-

https://doi.org/10.1021/acs.inorgchem.3c03532
Inorg. Chem. 2024, 63, 1589−1606

Scheme 1. (a) Synthesis of Bis-pyrazole Complexes, (i) 3,5-R′$_2$-pzH (1 equiv), TlPF$_6$ (1 equiv), Acetone, 298 K, 6 h and (b) Schematic View of Atropisomers for 1b

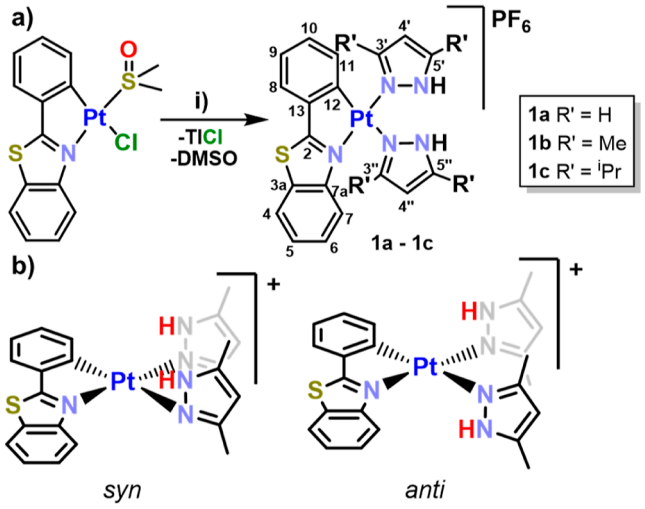

benzothiazole as a cyclometalating ligand [Pt(Me$_2$N-pbt)(R′$_2$-pzH)$_2$]PF$_6$ starting from [Pt(Me$_2$N-pbt)Cl(DMSO)] have been unsuccessful. In this case, the reactions evolve with formation of complex mixtures in which the chelating dimethylaminophenylbenzothiazole (Me$_2$N-pbt) deprotonates the coordinated pyrazoles, giving rise to mixtures with the corresponding bridging pyrazolate bimetallic complexes.

After a workup, complexes **1a−c** were obtained as yellow solids in good yields (85−90%) and were fully characterized (see Figures S1−S3). They show strong IR absorptions due to the PF$_6$ anion (ν 557, 841−845 cm^{-1}) and broad bands at 3363−3384 cm^{-1}, assigned to the tension frequency N−H of the pyrazole groups. The corresponding molecular peaks [Pt(pbt)-(R′$_2$pzH)$_2$]$^+$, found in the ESI(+) mass spectra of **1b** (m/z 597) and **1c** (m/z 709), and their molar conductivity (1:1 electrolytes) agree with the proposed stoichiometry. The presence of peaks related to the formation of [Pt$_2$(pbt)$_2$(pz)$_2$] in **1a** (m/z 967 [Pt$_2$(pbt)$_2$(pz)$_2$+Na]$^+$, 945 [Pt$_2$(pbt)$_2$(pz)$_2$ + H]$^+$, and 877 [Pt$_2$(pbt)$_2$(pz)]$^+$) suggests that this complex has a clear tendency to form the binuclear complex. The ^{1}H and ^{13}C{^{1}H} NMR spectra in CD$_3$COCD$_3$ show one set of signals corresponding to the cyclometalated group and nonequivalent R′$_2$pzH ligands. The assignment of the signals was made by ^{1}H−^{1}H (COSY and TOCSY) and ^{1}H−^{13}C (HSQC and HMBC) correlations. The more characteristic protons of the pbt ligand, H^7 and H^{11}, this last showing Pt coupling ($^3J_{Pt-H}$ ∼ 40 Hz), appear as doublets suffering an expected strong upfield shift [δ 6.18 (H^7) and 6.26 (H^{11}) **1a**, 6.26−6.19 (H^7 and H^{11}) **1b**, and 6.01 (H^7) and 6.15 (H^{11}) **1c**] compared to the precursor [Pt(pbt)Cl(DMSO)] [δ 9.62 (H^7) and 8.42 (H^{11})], due to the anisotropic shield of the aromatic pyrazole ligand. Bis-pyrazole compound **1a** displays a broad signal with Pt satellites assigned to the H$^{3'}$ (8.10 ppm, $^3J_{Pt-H}$ 20.3 Hz), whereas the derivatives **1b−1c** show the corresponding signals of the alkyl substituents on the pyrazole co-ligands in the aliphatic region. Complexes **1a** and **1c** show two broad singlets at low frequencies due to the N−H protons of the pyrazole groups, whereas complex **1b** displays four signals indicating the presence of two conformational isomers in a *ca* 35:65 molar ratio. We note that in these complexes there are two possible relative orientations of the NH units of the pyrazole ligands in relation to the platinum coordination plane leading to a *syn/anti* isomerism (Scheme 1b). In complex **1b**, the interconversion between both conformers (atropisomers) seems to be slower than the NMR time scale. The presence of both conformers is also apparent in the H$^{4',4''}$ protons (δ 6.40−6.28 range, 2H) and methyl resonances (2.47−2.35 ppm, 2H) of the nonequivalent 3,5-dimethylpyrazole ligands and in the corresponding ^{13}C{^{1}H} NMR signals (See Figure S2). Finally, **1a−1c** complexes display the expected doublet (∼−72.6 ppm, $^1J_{F-P}$ 706 Hz) and septuplet (∼−145 ppm) in the ^{31}P{^{1}H} and ^{19}F{^{1}H} NMR spectra, respectively, corresponding to the PF$_6$ counteranion.

Table 1. Selected Bond Distances (Å) and Angles (deg) of 1a·PO$_2$F$_2$, 1b, 2a, 3a·THF, 4a, and 5a·0.5CH$_2$Cl$_2$

parameter	1a·PO$_2$F$_2$	1b	2a	3a·THF	4a	5a·0.5CH$_2$Cl$_2$
Pt-C$_{C^N}$	2.01(2)	2.007(10)	2.001(3)	2.001(6)	2.013(2)	2.012(6)
			1.998(3)	1.993(6)		2.012(7)
Pt-N$_{C^N}$	2.042(16)	2.038(8)	2.036(2)	2.043(5)	2.052(2)	2.055(5)
			2.033(2)	2.039(5)		2.049(6)
Pt-N$_{pyr(trans\text{-}C)}$	2.08(2)	2.117(9)	2.099(2)	2.103(5)	2.118(2)	2.146(5)
			2.090(2)	2.105(5)		2.137(6)
Pt-N$_{pyr(trans\text{-}N)}$	1.960(18)	2.002(9)	1.989(2)	2.004(5)	2.0038(19)	2.001(6)
			2.000(2)	1.998(5)		2.003(6)
Pt-Pt			3.344	3.1740(4)	2.58972(19)	
Pt-Cl					2.4177(6)	2.4304(15)
						2.4112(19)
C$_{C^N}$-Pt- N$_{pyr}$	94.9(9)	92.6(4)	95.80(10)	95.0(2)	93.73(9)	91.4(2)
			95.80(11)	95.0(2)		92.2(3)
C$_{C^N}$-Pt- N$_{C^N}$	80.4(9)	80.8(4)	80.76(10)	81.6(2)	80.83(9)	80.9(2)
			80.92(11)	81.1(2)		80.8(3)
N$_{C^N}$-Pt- N$_{pyr}$	97.1(8)	99.2(3)	99.50(9)	98.7(2)	99.73(8)	102.3(2)
			98.42(9)	99.0(2)		100.8(2)
N$_{pyr}$-Pt- N$_{pyr}$	87.7(8)	87.45(3)	84.16(9)	84.8(2)	84.32(8)	84.0(2)
			84.72(9)	85.0(2)		84.3(2)
Cl-Pt-Pt					162.894(14)	165.71(6)
						166.71(6)

https://doi.org/10.1021/acs.inorgchem.3c03532
Inorg. Chem. 2024, 63, 1589−1606

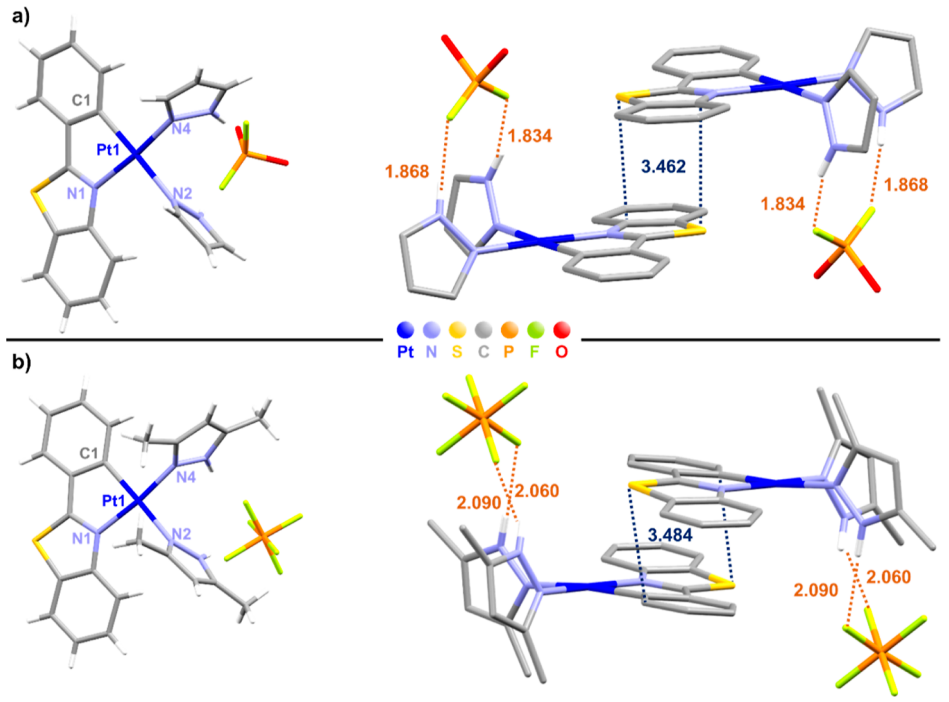

Figure 1. Molecular structure and crystal stacking of complexes **1a**·PO_2F_2 (a) and **1b** (b).

Scheme 2. Synthesis and Conditions for the Preparation of Pt_2^{II} Derivatives; (i) NEt_3 (exc.), Acetone, 8 h; (ii) Hpz (1 equiv), $TlPF_6$ (1 equiv), NEt_3 (exc.), Acetone, 6 h; and (iii) Hpz (1 equiv), KOH (exc.), EtOH/Acetone, 24 h[a]

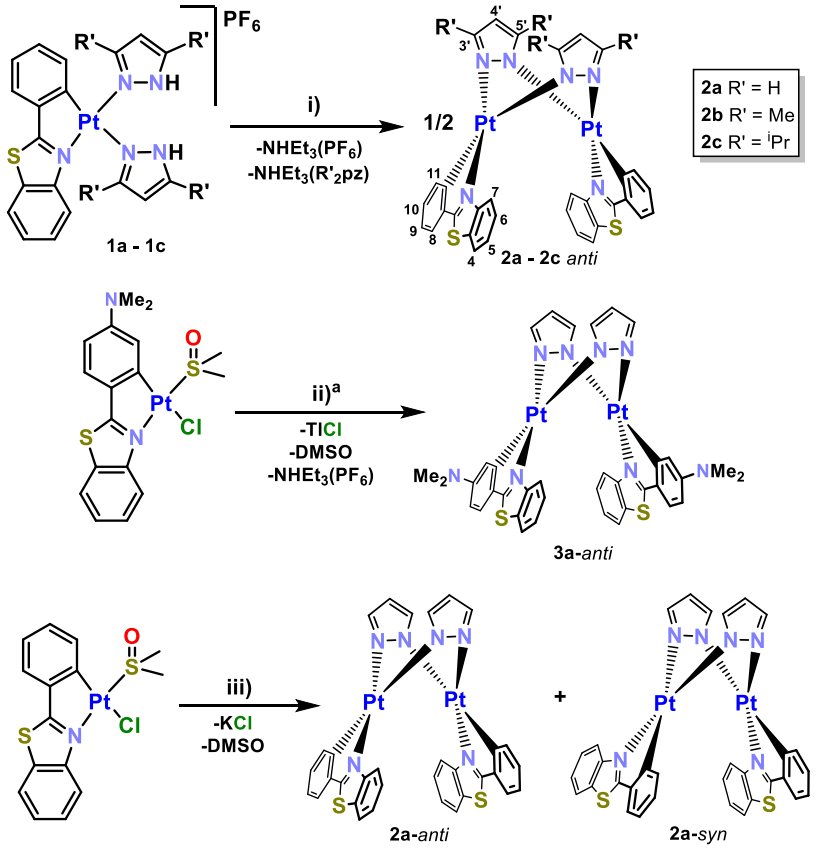

[a]The isomer **3a**-*anti* was also obtained using via (iii).

Suitable crystals for complexes **1a** and **1b** have been obtained by slow diffusion of *n*-hexane through a solution of the corresponding compound in acetone at low temperatures. In the case of **1a**, the X-ray diffraction study (Tables 1, S1 and S2) revealed that this complex crystallized with the PO_2F_2 anion generated by the partial hydrolysis of the PF_6^- group (**1a**·

https://doi.org/10.1021/acs.inorgchem.3c03532
Inorg. Chem. 2024, 63, 1589−1606

PO_2F_2). Hydrolysis of the PF_6^- anion has been previously observed.[17f] A view of the molecular structures with the selected bond lengths and angles and a vision of the interaction of the cation and the anions is presented in Figure 1. Both cations showed the expected chelate C^N coordination of the pbt ligand and the *cis* arrangement of the two R′$_2$-pzH ligands. The bite angle of the pbt ligand [80.4(9)° **1a·PO_2F_2**, 80.8(4)° **1b**] and the Pt−C(1) [2.01(2) **1a·PO_2F_2**, 2.007(10) Å **1b**] distance (Table 1) are within the expected values for this type of complexes.[24] The Pt−N(2) distance [2.08(2) **1a·PO_2F_2**, 2.117(9) Å **1b**] *trans* to the C-metalated is longer than the Pt−N(4) distance [1.960(18) **1a·PO_2F_2**, 2.002(9) Å **1b**] (Table 1), reflecting the high *trans* influence of the metalated carbon. The phenyl benzothiazole ligand is almost coplanar with respect to the Pt coordination plane (deviations 2.60° **1a·PO_2F_2**, 7.56° **1b**). In the crystal, the pyrazole ligands display a *syn* orientation, which is stabilized by the occurrence of short hydrogen bonding interactions between the NH protons and the fluorine atoms of the counteranion. The F···H distances are shorter in **1a·PO_2F_2** than in **1b** (1.868, 1.834 Å **1a·PO_2F_2** vs 2.090, 2.060 Å **1b**) and within the range reported for F···H bonding interactions.[25] Both complexes form dimers through moderate intermolecular $\pi\cdots\pi$ (pbt···pbt, 3.462 **1a·PO_2F_2** and 3.484 Å **1b**) interactions (Figure 1).

Synthesis and Characterization of Bis(pyrazolate) Diplatinum Complexes. The binuclear pbt−platinum complexes with pyrazolate bridging ligands [Pt(pbt)(μ-R′$_2$pz)]$_2$ (R′$_2$-pz = pz **2a**, 3,5-Me$_2$pz **2b**, 3,5-^{i}Pr$_2$pz **2c**) were prepared by the reaction between the corresponding bis-pyrazole [Pt(pbt)(R′$_2$-pzH)$_2$]PF_6 (**1a−1c**) with excess of NEt_3 at room temperature (Scheme 2i). The related 2-(4-dimethylaminophenyl)-benzothiazole derivative [Pt(Me$_2$N-pbt)(μ-pz)]$_2$ **3a** was also prepared by reaction of [Pt(Me$_2$N-pbt)Cl(DMSO)] with 1 equiv of Hpz, $TlPF_6$, and NEt_3 (see Scheme 2ii) or by using Hpz (1 equiv) and excess of KOH (see the Supporting Information for details). Following these pathways, the binuclear complexes were selectively obtained as the *anti*-isomers. Complex **2a** was also prepared starting from the mononuclear complex [Pt(pbt)-Cl(DMSO)], by using Hpz (1 equiv) and excess of KOH (Scheme 2iii). However, in this case, the reaction evolves with formation of a mixture of the isomers **2a**-*anti* and **2a**-*syn* in relation ∼5:1, as assessed by ^{1}H NMR spectroscopy.

The bimetallic nature of the complexes was supported by ESI(+) or MALDI(+)-MS analysis, as they show as the parent peak, the corresponding one due to $[M + H]^+$ (m/z 945 **2a**, 1000 **2b**, 1112 **2c**, and 1030 **3a**) (Section S3 and Experimental Section in the Supporting Information). Unfortunately, only complexes **2a** and **3a** are soluble enough in THF-d^8 to characterize them by ^{1}H NMR spectra. The *anti*-isomers (*anti*- **2a** and **3a**) exhibit the presence of only one set of pbt ligands together with one set of pyrazolate groups. In both complexes, the most deshielded signal corresponds to the H^7 of the pbt, which appear as a doublet (δ 7.89 **2a**-*anti*, 7.74 **3a**), whereas the most shielded is attributed to the H$^{4'}$ of bridging pyrazolate (δ 6.34 **2a**-*anti*, 6.3 **3a**) (Supporting Information, Section S2). In the *anti*/*syn*-**2a** mixture, the most distinct signal of the type of isomer corresponds to the H$^{4'}$ of the pyrazolate, which are equivalent for the *anti*-**2a** isomer (δ 6.34) and inequivalent in the *syn*-**2a** (δ 6.48; 6.32) (Figure S4b). Suitable yellow crystals for X-ray studies of *anti*-**2a** and **3a·THF** were obtained from slow evaporation of a THF solution. Their molecular structures are depicted in Figures 2 and S11, and the corresponding structural bonding details are provided in Tables 1 and S2. The structures

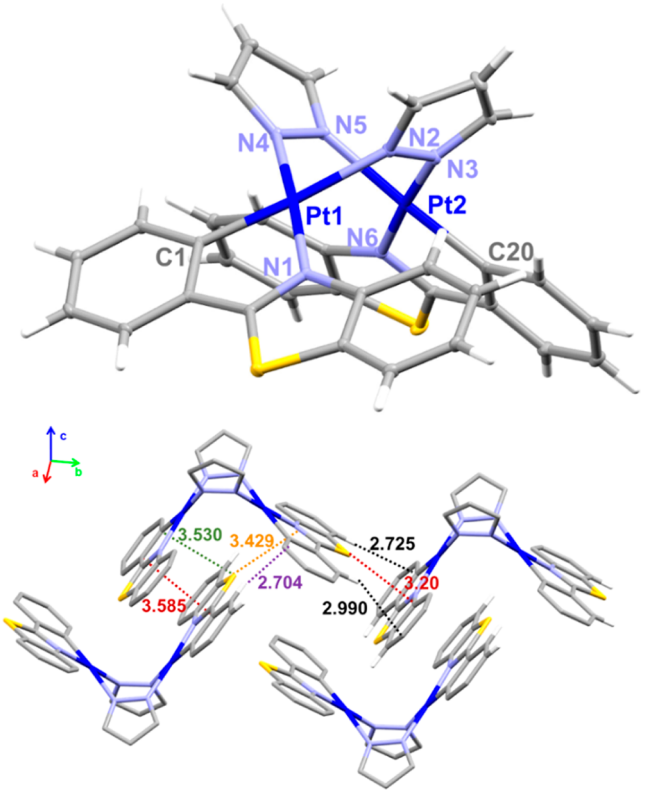

Figure 2. Molecular structure and crystal packing of complex **2a**.

confirm the *anti*-arrangement of the Pt(R-pbt) units bridged by the two pyrazolate ligands, in coherence with the NMR spectra. Both Pt^{II} complexes display the typical butterfly-like structure with a C_2 symmetry. The intermetallic distances [3.344 **2a** and 3.1740(4) Å **3a**, Table 1] are shorter than the sum of the van der Waals radii of the two Pt (3.5 Å) and comparable to those found in related μ-pyrazolate diplatinum complexes (2.834−3.486 Å).[12,26] It has been previously shown that in this type of complexes, both the Pt···Pt distance and the tilt angle decrease due to the increasing demanding of the substituents of the bridging pyrazolate ligand (3- and 5-positions).[26d] Also the bulkiness of the cyclometalating group affects to the proximity of the platinum fragments in these type of binuclear complexes.[27] Surprisingly, despite the presence of bulky NMe$_2$ groups in **3a**, the Pt···Pt is shorter and the angle between platinum planes is smaller than in **2a** (84.23° for **2a** and 73.50° for **3a**), indicating stronger interactions between the platinum fragments, a fact that might be attributed to the coplanarity between the NMe$_2$ and the bt unit. On the basis of previous results, it is suggested that the Pt···Pt separation could likely be shorter in complex **2b** (R′ = Me) and, particularly, in **2c** featuring R′ = Pr^i groups, what agrees with their intense orange colors. The Pt−C and Pt−N bond distances around the Pt centers are similar to those found in related complexes. In particular, the Pt−N$_{pz}$ distance *trans* to the C$_{R\text{-}pbt}$ [2.099(2) **2a** and 2.103(5) Å **3a**] is longer than that of *trans* to the N of the R-pbt group [2.000(2) **2a** and 2.004(5) Å **3a**] (Table 1), in coherence with the high *trans* influence of the metalated carbon. The extended structure of both compounds shows weak $\pi\cdots\pi$ interactions between cyclometalated groups of different molecules giving rise to dimers (3.585−3.641 Å) supported by secondary *intermolecular* sulfur···carbon (S$_{R\text{-}pbt}$···C$_{R\text{-}pbt}$ ∼ 3.43 Å) and C−H···π (2.704−2.971 Å) interactions. These dimers additionally stack giving rise to a 1D infinite

https://doi.org/10.1021/acs.inorgchem.3c03532
Inorg. Chem. 2024, 63, 1589−1606

Scheme 3. Synthesis and Conditions of Binuclear Bis-pyrazolate Pt_2^{III} Complexes; (i) $CHCl_3$, Sunlight, 298 K, 24 h or $PhICl_2$, CH_2Cl_2, 0 °C, 8 h

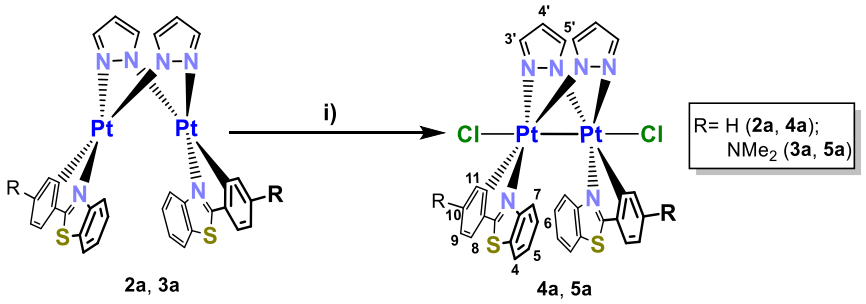

arrangement supported by C−H···π (2.778−2.836 Å) and ($S_{R\text{-}pbt}$···$C_{R\text{-}pbt}$ ∼ 3.20 Å) (Figures 2 and S11).

We observed that complexes $[Pt(R\text{-}pbt)(\mu\text{-}pz)]_2$ (R = H **2a**, Me_2N **3a**) are stable in $CHCl_3$ solution in the dark, but in the presence of sunlight they evolve slowly (∼24 h) to form the metal−metal-bonded Pt^{III}−Pt^{III} complexes $[Pt(R\text{-}pbt)(\mu\text{-}pz)\text{-}Cl]_2$ (**4a**, **5a**), which precipitate in the mixture in a *ca* yield of 60%. This type of two center-two electron oxidation reactions have been previously studied and depend on many factors involving either a radical-like mechanism (with the O_2 acting as a radical R* trap) and/or a thermally or photochemically activated processes.[26h,28] Recent studies on pyrazolate- and thiolate-bridged diplatinum complexes with very short Pt···Pt distances indicate that the ^{1}MMLCT excited states easily triggers the photooxidation of these complexes with $CHCl_3$.[10b] As expected, the complexes were also obtained by reacting **2a** and **3a** with iodobenzenedichloride ($PhICl_2$) in CH_2Cl_2 at 0 °C, being precipitated and separated of the mixture in a 59−73% yield (Scheme 3). Complexes **4a** and **5a** have been characterized by mass spectrometry and NMR spectroscopy (Experimental Section and Sections S2 and S3 in the Supporting Information) and their structures confirmed by X-ray. The formation of the oxidized species is evident by the presence of peaks due to $[M\text{-}Cl]^+$ (*m*/*z* 979 **4a**, 1065 **5a**) as parent peaks in their mass spectra.

The ^{1}H NMR spectra of **4a** and **5a** display only one set of signals for the R-pbt groups and for the pyrazolate ligands, indicating an *anti*-arrangement of the cyclometalated group. The *ortho* protons to the cyclometalated ligand, H^{11}, are notably shielded and the three-bond platinum-coupling constant ($^3J_{Pt-H}$ 31.1 **4a**, 35.2 Hz **5a**) is smaller than in complex **1a** (43.3 Hz), in agreement with the increased oxidation state. The molecular structures of complexes **4a** and **5a·0.5CH_2Cl_2** were determined by single-crystal X-ray diffraction (Table 1 and Figures 3 and S12). The Pt^{III}−Pt^{III} complexes retain the boat-like structure of the Pt_2N_4 core and the *anti*-arrangement of the platinum(C^N) fragments. The interplanar angles between the platinum coordination planes are notably reduced with respect to those observed in Pt^{II}−Pt^{II} precursors (35.68° **4a** and 34.30° **5a** vs 84.23° **2a** and 73.50° **3a**) due to the formation of the Pt−Pt bond. Each Pt^{III} center shows a distorted octahedral coordination environment with axial positions occupied by chloride atoms and the other Pt^{III} center, with angles Cl−Pt−Pt of 162.894(14)° for **4a** and 165.71(6)° and 166.71(6)° for **5a** (Table 1), similar to those reported for related complexes.[12,26h] As expected, the formation of a Pt−Pt formal bond produces a shortening in the Pt−Pt distance with respect to complexes **2a** and **3a** [2.5897(2) **4a** 2.5776(3) Å **5a** vs 3.344 **2a**, 3.1740(4) Å **3a**, Table 1]. The molecular packing of these complexes shows extended π···π interactions through the R-pbt groups with distances of 3.458−3.544 Å in **4a** and 3.416−3.538 Å for **5a**, forming 1D chains (Figures 3 and S12).

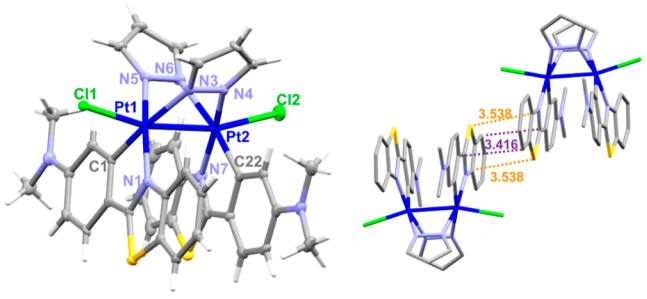

Figure 3. Molecular structure and crystal packing of **5a·0.5CH_2Cl_2**.

Optical Properties. *Absorption Properties and TD-DFT Calculations.* The UV−vis spectra of bis(pyrazole) complexes **1a**−**1c** in THF (5×10^{-5} M) solution and in the solid state (Table S3, Figures 4 and S13a) are rather similar, indicating a negligible influence of the pyrazole groups. In solution, they show one intense absorption at ca. 260 nm, attributed to spin-allowed π−π* intraligand (^{1}IL, pbt) transitions. They exhibit an additional band in the 300−370 nm range and a less intense feature in the low-energy region at 385−420 nm ($\varepsilon \sim 10^3$ L·mol^{-1}·cm^{-1}). On the basis of theoretical calculations carried out in complex **1a** (Figure 4 and Section S5, Supporting Information), which indicate that the calculated low energy transition (S_1 382 nm) is mainly contributed by the HOMO (80% pbt, 20% Pt) to LUMO (93% pbt, 6% Pt) excitation, the low-energy feature is mainly attributed to an intraligand ^{1}IL (pbt) with some ^{1}MLCT. The band in the range of 300−370 nm has also a mixed ^{1}MLCT/^{1}IL character. The Hpz orbitals contribute from the LUMO+1 (63%) and they are involved in the S_6/S_8 transitions with very low oscillator strength (Table S4 and Figure S15).

As noted, the binuclear Pt^{II}−Pt^{II} complexes **2b** and **2c** are insoluble in common solvents. Therefore, only the absorption spectra of the pyrazolate bridging complexes **2a** and **3a** could be recorded in THF solution (Figure 5). In both compounds, the band at λ < 350 nm are ascribed to π−π* intraligand (^{1}IL, pbt) and ligand-to-ligand (R_2pz to pbt) transitions. In **2a**, the bands between 350 and 410 nm are ascribed to mixed ^{1}IL/^{1}MLCT and the low energy feature at *ca*. 440 nm to ^{1}MMLCT transitions, as supported by calculations (see Table S4). In the Me_2N-pbt **3a**, the bands are more intense indicating a stronger intraligand charge-transfer contribution (NMe_2 to bt) and are slightly red-shifted (**3a** 430, 450 nm $\varepsilon \sim 20 \times 10^3$ vs **2a** 384, 440 nm ε 4.78 × 10^3). As seen in Figure 5, which shows the frontier orbitals for

https://doi.org/10.1021/acs.inorgchem.3c03532
Inorg. Chem. 2024, 63, 1589−1606

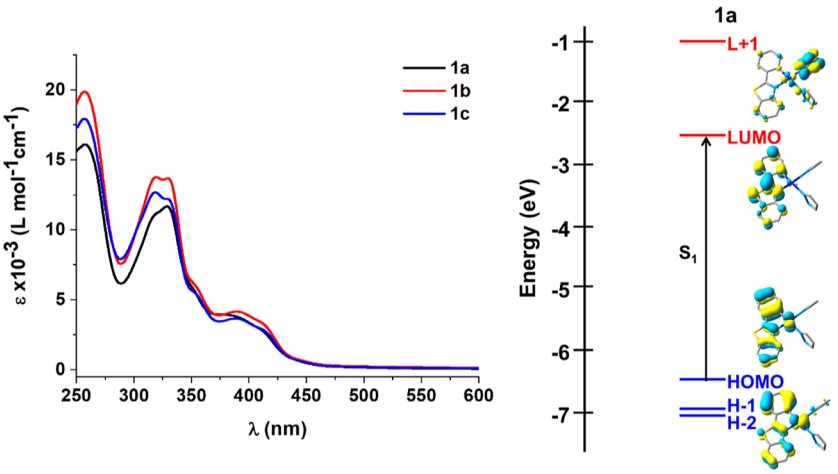

Figure 4. UV−vis absorption spectra of mononuclear complexes **1** and schematic representation of selected orbitals frontiers and transitions for **1a**.

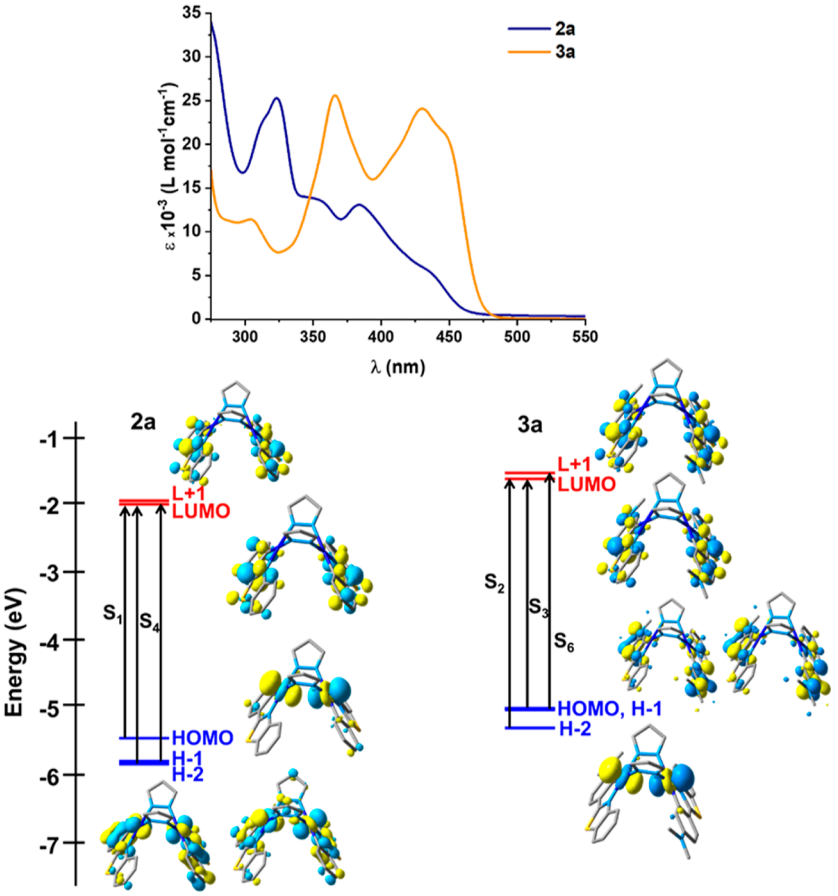

Figure 5. UV−vis absorption spectra of mononuclear complexes **2a** and **3a** in THF (5×10^{-5} M) and an schematic representation of their frontier orbitals and selected excitations.

both complexes, in both, the target LUMO and L+1 spread on the cyclometalated ligands. However, whereas in **2a**, the highest orbital HOMO has a σ^* ($5d_{z^2}-5d_{z^2}$) character and is located on the two platinum atoms; in **3a**, a similar orbital is the H-2. In **3a**, the HOMO and HOMO−1 are destabilized in relation to **2a** and are located on the Me_2N-pbt. For **2a**, the calculated S_1 (452 mn) and S_2 (439 nm) have ^{1}MMLCT characters, whereas for **3a** the most intense calculated absorptions are S_2 (423 mn) and S_3 (415 nm) and have mixed ^{1}ILCT/^{1}MMLCT. It is interesting to note that in both complexes the calculated transitions with remarkable metal platinum contribution and mixed ^{1}MLCT/^{1}ILCT character appear at higher energy (S_4 397 nm **2a**; S_7 351 nm **3a**). The solid-state absorption spectra of **2a**−**2c** have been also recorded. The main lowest-energy band ranges from 438 (**2a**), 455 (**2b**) to 503 nm (**2c**), with extending tails, in agreement with their color (Table S3 and Figures S13, S14), what are ascribed to mixed ^{1}IL/^{1}MMLCT, with higher contribution of this latter on going from **2a** to **2c**, likely due to a lower Pt−Pt distance by increasing the steric bulk of the substituents. Low intense features in the tails (>480 nm **2a**, **2b** or

https://doi.org/10.1021/acs.inorgchem.3c03532
Inorg. Chem. 2024, 63, 1589−1606

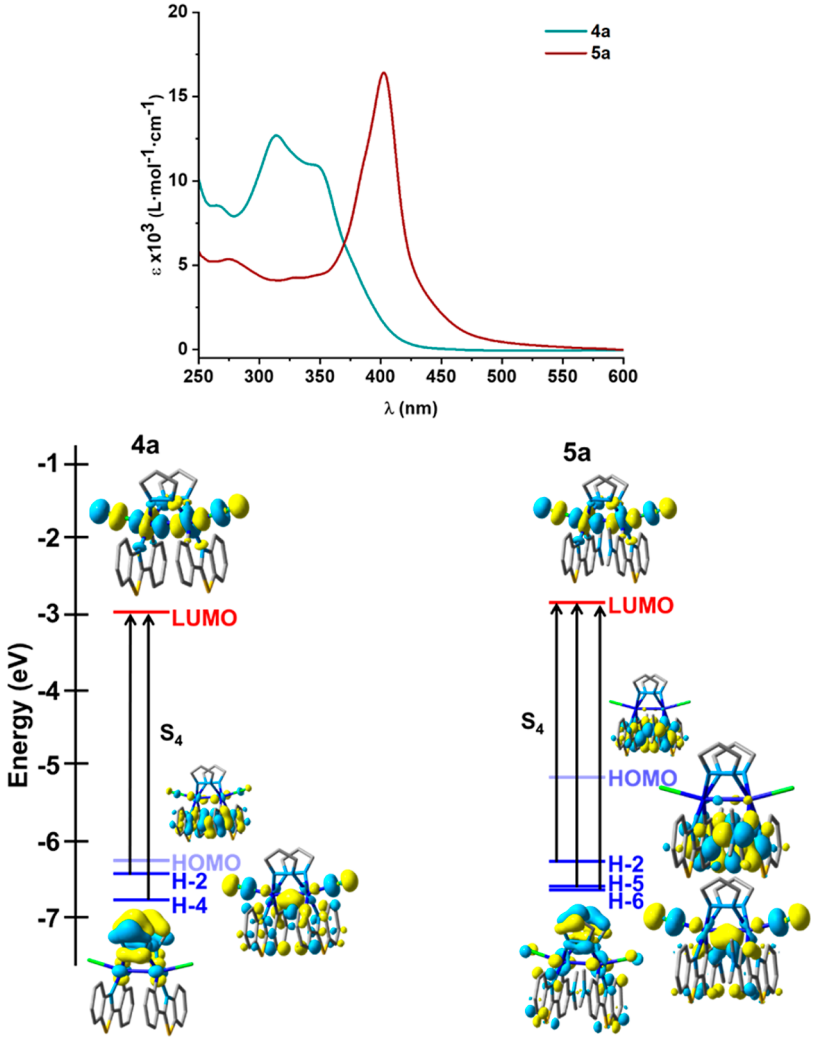

Figure 6. UV−vis absorption spectra in THF solution (5×10^{-5} M) of **4a** and **5a** and an schematic representation of their frontier orbitals and selected excitations.

Table 2. Photophysical Data for Complexes 1a−1c and 2a and 3a in THF Solution (5×10^{-4} M)[a]

	298 K						77 K
compound	λ_{em}/nm	φ[b]	φ[c]	τ[d]/μs	k_r[e]/s^{-1}	k_{nr}[f]/s^{-1}	λ_{em}/nm
1a[g]	543, 577$_{max}$, 620	0.10	0.01	4.5	2.2×10^4	2.0×10^5	529, 569$_{max}$, 618
1b[g]	540, 576$_{max}$, 620	0.20	0.02	5.7	3.5×10^4	1.4×10^5	526, 567$_{max}$, 616
1c[g]	534, 573$_{max}$, 617	0.21	0.03	5.2	4.0×10^4	1.5×10^5	527, 568$_{max}$, 615
2a[g]	550, 589$_{max}$, 634	0.01	0.01	0.9	1.1×10^4	1.1×10^6	544, 585$_{max}$, 634
3a[g]	405$_{max}$, 570, 614[b,g]	0.23[g] / 0.17[h]	<0.01[g] / 0.02[h]	0.0016 [405]	2.6×10^4[g] / 2.0×10^4[h]	8.9×10^4[g] / 9.5×10^4[h]	565$_{max}$, 609
	500, 570$_{max}$, 614[b,h]			0.0015 [500]			
	500, 570$_{max}$, 614[c,h]			8.7 [570]			

[a] λ_{ex} 365−450 nm. [b] Deoxygenated. [c] Oxygenated. [d] λ_{ex} 390 nm(LED). [e] $k_r = \phi/\tau_{average}$. [f] $k_{nr} = (1 - \phi)/\tau_{average}$ in deoxygenated conditions. [g] λ_{ex} 365 nm. [h] λ_{ex} 400−450 nm.

540 nm, **2c**) are observed, which are probably of spin-forbidden nature.

The absorption spectra of Pt^{III}−Pt^{III} **4a** and **5a** are included in Figure 6. The most significant feature in relation to complexes **2a** and **3a** is the notable hypsochromic shift in the low energy region. Thus, **4a** displays a moderately intense absorption low energy band at 348 nm with a shoulder at 379 nm and **5a** a band at 402 with a shoulder at 444 nm, clearly blue-shifted in relation to the corresponding Pt^{II}−Pt^{II} (440 **2a**, 430 nm **3a**), reflecting to the oxidation of the platinum centers and the notable change in the frontier orbitals. DFT and time-dependent DFT (TD-DFT) calculations were performed with the Gaussian 16 program package to explore the orbital frontiers and the nature of the excited states and transitions (Tables S4−S7 and Figure S16). Figure 6 includes a selection of the orbitals and excitations. In both complexes, the LUMO is essentially identical located on

https://doi.org/10.1021/acs.inorgchem.3c03532
Inorg. Chem. 2024, 63, 1589−1606

the ClPtPtCl axis and formed by the antisymmetrical σ^* combination of the $5d_{z^2}$ of the two platinum centers and the p_z orbitals of the chloride atoms (58% Pt−Pt and 26% Cl−Cl). Therefore, population of this orbital should cause strong distorted excited states with elongation of the Pt−Pt separation and of the Pt−Cl bonds. The symmetrical combination σ of the $5d_{z^2}$ is mainly located on the HOMO−2, but this orbital has also a notable contribution of the phenylbenzothiazolate groups. For complex **5a**, the HOMO and H-1 are primarily located on the Me_2N-pbt groups, while in the pbt complex, **4a** have also small platinum and Cl contributions (see Table S7). The calculated low lying S_1-S_3 (431 to 489 nm **4a** and 748−489 nm **5a**) transitions have very low oscillator strength and complex configuration (mixed LMMCT/LXCT/L'XCT **4a** and LMMCT/LXCT/ILCT **5a**) (L = R-pbt, X = Cl, L' = pz). The most intense low energy-calculated band is S_4 ascribed to H-4, H-2 to LUMO in **4a** and to a more complex configuration in **5a** (H-2, H-5, H-6, and H-10 to LUMO) having a mainly L'MMCT/L'XCT nature in **4a** and LMMCT/L'MCT/XC/MC in **5a**. The solid-state spectra also reflect the oxidation of the Pt centers exhibiting blue-shifted low-energy features in relation to the $Pt^{II}-Pt^{II}$ precursors (see Table S3, Figure S14).

Emission Properties and DFT Calculations. The emission spectra of complexes **1** and **2a**−**5a** were registered in THF fluid solution (5×10^{-4} M for **1** and **2a**−**3a** and 5×10^{-5} M for **4a**), THF glasses at 77 K, polystyrene (PS) films at 10% wt, and in the solid state for all complexes at room and low temperatures (Tables 2 and S8, Figures 7−10 and S17−S19). Mononuclear

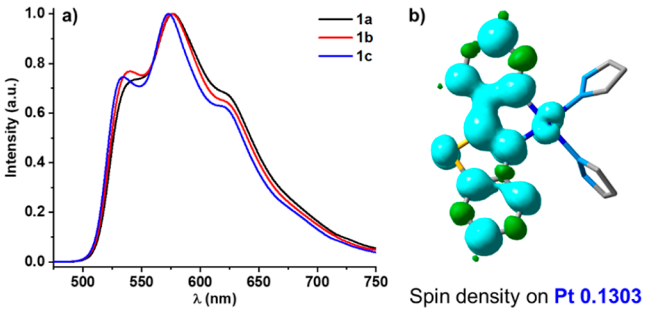

Figure 7. (a) Emission spectra (λ_{ex} 420 nm) of complexes **1** in THF solution (5×10^{-4} M) at 298 K and (b) spin density surface on T_1 state of complex **1a**.

complexes **1a**−**1c** show in the solid state, THF solution and doped films at 298 K a similar long-lived vibronically structured emission band (λ_{max} ~ 540 nm), slight blue-shifted at low temperatures (λ_{max} ~ 530 nm), attributed to a predominant intraligand transition (^{3}IL) with some metal-to-ligand charge-transfer (^{3}MLCT) characters. This emission is comparable to those reported for related neutral heteroleptic monomers [Pt(pbt)(L^X)] (L^X = O^O, N^O, P^O),[4d,17e,29] and the assignment is further supported by optimization of the triplet excited (T_1) state for complex $\mathbf{1a}^+$. As illustrated in Figure 7, the spin density surface at the optimized T_1 state is centered on the pbt ligand with some contribution of the platinum (Pt ~ 0.13). The adiabatic calculated emission wavelength (638 nm) exhibits the expected overestimated value in relation to the experimental data (~540 nm, THF, 298 K). The calculated quantum yields are moderate in solution (10−21%, deoxygenated conditions, Table 2) but relatively low in rigid media (solid and PS, 1−8% Table S8), indicating aggregation-caused quenching characteristics (ACQs).[30] The relatively strong $\pi\cdots\pi$ and S$\cdots\pi$ interactions between the pbt ligands in these rigid media, as found in their X-ray structures, could provide easy deactivation pathways and may account for the reduced efficiencies. Notwithstanding, it is worth noting that reports on luminescent mononuclear bis-pyrazole Pt^{II} complexes are rare.[31] A comparison of the radiative and nonradiative rate constants (k_r and k_{nr}) reveals that complex **1a** presents the highest k_{nr} value in relation to **1b** and **1c** (k_{nr} 2×10^5 **1a** vs 1.4×10^5 **1b**, and 1.5×10^5 **1c**) and the lowest k_r (2.2×10^4 **1a** vs 3.5×10^4 **1b** and 4×10^4 **1c**), resulting in a less efficient phosphor (φ 10% **1a** vs 20% **1b** and 21% **1c**). This could be associated with a less steric hindrance of the pyrazole ligand in **1a**, which provides less rigidity.

The bimetallic complex **2a** displays in all media a well-resolved vibronic emission profile with λ_{max} (~540−550 nm) (Figure 8), close to that observed for complexes **1**, being therefore ascribed to a local mixed ^{3}IL/^{3}MLCT excited states. This behavior could be related to the relatively long Pt···Pt of 3.344 Å distance found for this complex, which makes it difficult to reach the σ^2-σ^{*1} configuration characteristic of the ^{3}MMLCT excited state.[10a,11b,26k] The optimized S_0 structure for complex **2a** shows a Pt−Pt separation of 3.2069 Å, comparable to that found in the crystal structure, and similar separation is found in the optimized T_1 excited state (see Table S5), indicating the absence of short intramolecular platinum−platinum bonding interaction typical of the ^{3}MMLCT excited state in T_1. To confirm the nature of the emission, the lowest T_1-T_3 vertical excitations at the S_0 geometry and the corresponding optimized T_1-T_3 were calculated (Tables S4, S9, S10 and Figure 8b). The two lowest vertical triplet excitations $T_{1,2}$, which are close in energy (2.4 and 2.5 eV), and their corresponding optimized $T_{1,2}$ states (676 nm) are located on one of the Pt(pbt) fragments having mixed ^{3}IL/^{3}MLCT nature. As illustrated in Figure 8b, the following excitation, T_3, has a ^{3}MMLCT character but is located at 0.3 eV above T_1. In **2a**, the metal contribution in T_1 increases in relation to the mononuclear complex **1a** (0.2125 **2a** vs 0.1303 **1a**, Table S9) pointing to a higher metal-to-ligand charge-transfer (^{3}MLCT) contribution in **2a**, in correlation with the lower lifetime recorded in THF solution for this bimetallic complex in comparison to the **1a** one (4.5, **1a** vs 0.9 μs, **2a**). The recorded quantum yield for **2a** in deoxygenated THF solution (1%) is lower than for **1a** (10%), but relatively similar in solid and PS (Table S8). This decrease in the quantum efficiency is attributable to an appreciable increase in k_{nr} (1.1×10^6 **2a** vs 2.0×10^5 **1a**), while there is a decrease in k_r (1.1×10^4 **2a** vs 2.2×10^4 **1a**).

For complexes **2b** and **2c**, only emission properties in the solid state were recorded (Figure 8c,d). Dimethylpyrazolate-bridge derivative (**2b**) shows, at room temperature and at 77 K, a similar band to that obtained for complex **2a** (~550 nm) indicating emission from an ^{3}IL/^{3}MLCT excited state. For complex **2c**, with a bulkier substituent on the bridge group (R = ^{i}Pr), the emission is broader at 298 K peaking at 560 nm and well stylized and red-shifted to 600 nm at 77 K (Figure 8d). This fact suggests the contribution of the low lying ^{3}MMLCT excited state, which becomes predominant by decreasing the temperature.

Complex **3a**, comprising the donor−acceptor Me_2N-pbt groups, displayed a significantly different behavior from that of the related complex **2a** (Table 2). It exhibits, upon excitation on the low energy band at 400−450 nm, and in a carefully deoxygenated THF solution at 298 K, in addition to a strong long-lived low energy band (LE) in the yellow-orange region (570 nm), a minor high energy feature (HE) in the blue-green

https://doi.org/10.1021/acs.inorgchem.3c03532
Inorg. Chem. 2024, 63, 1589−1606

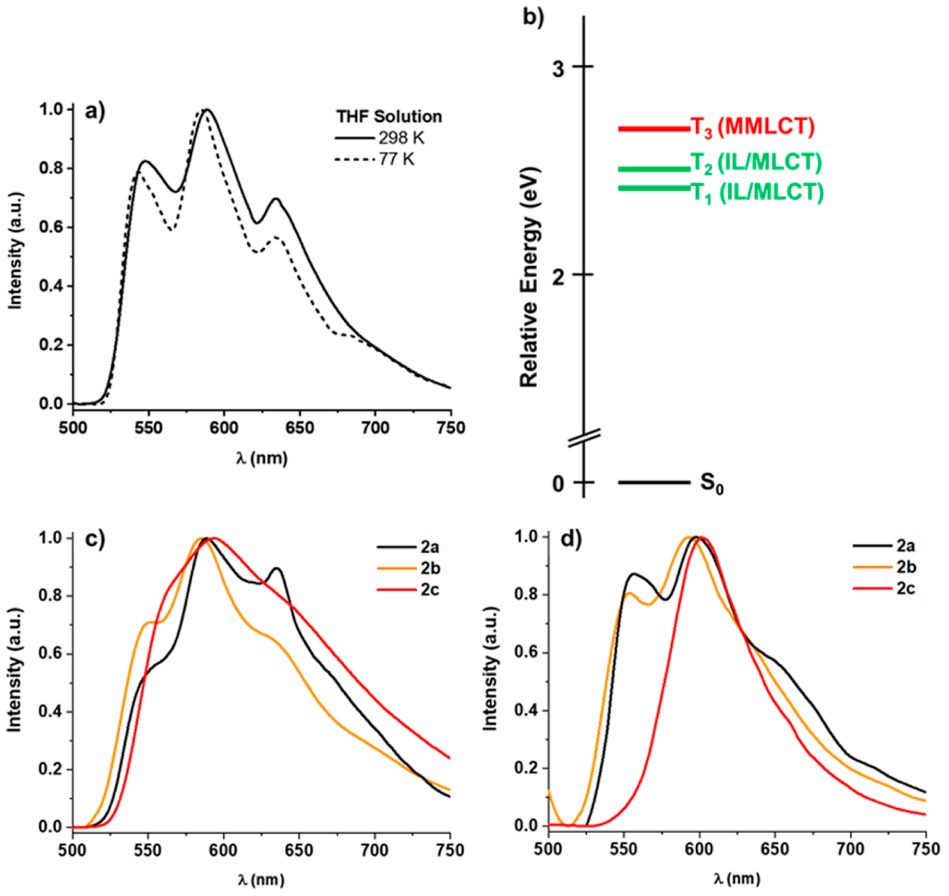

Figure 8. (a) Emission spectra (λ_{ex} 400−450 nm) of complex **2a** in THF solution at 298 and 77 K. (b) Relative energies and character of the vertical triplet excitations (T_1−T_3) for complex **2a**. Emission spectra of **2a**−**c** in solid state (c) at 298 (d) at 77 K.

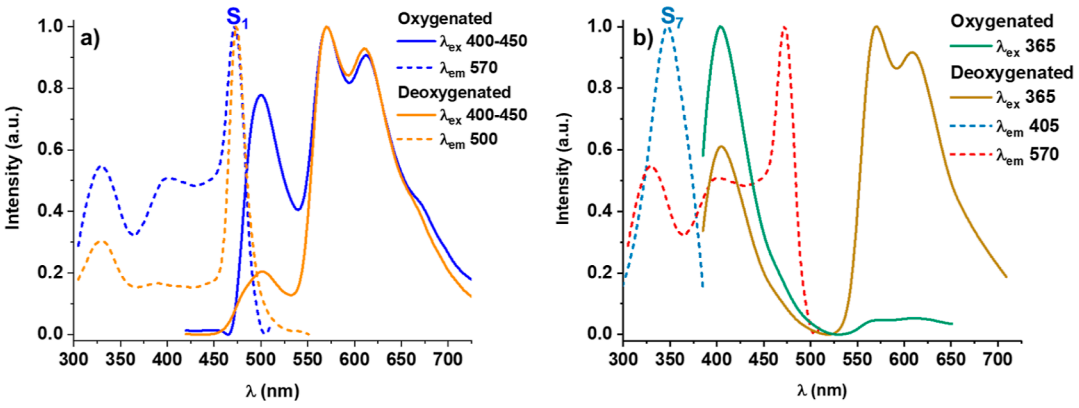

Figure 9. Excitation (····) and emission (—) spectra of complex **3a** in oxygenated and deoxygenated THF 5×10^{-4} M solution at 298 K upon excitation at (a) 400−450 and (b) 365 nm.

region (500 nm) (see Figure 9a, orange line). The high energy feature is short-lived (1.5 ns) and displays characteristic mirror band-shaped with the longest wavelength absorption band, being therefore ascribed to $S_1 \rightarrow S_0$ fluorescence having metal-perturbed intraligand charge-transfer ^{1}ILCT (Me_2Nph-to-bt) characters, whereas the LE-structured phosphorescent band is ascribed, according to calculations, to ^{3}ILCT. In this complex **3a**, the two first triplet excitations $T_{1,2}$ at the S_0 geometry are essentially isoenergetic (556 nm) and exhibit an ILCT character (Figure 10c). The T_3, with a MMLCT character, lies more separated from T_1 (0.6 eV) than in **2a** (0.3 eV). The spin density distribution on the optimized T_1 is mainly located on one of the cyclometalated groups with a lower metallic contribution in relation to the pbt-derivative **2a** (0.0809 **3a** vs 0.2125 **2a**), supporting primarily ^{3}ILCT nature for the phosphorescent emission (Table S9). As was expected, the ratio F/P clearly increases in oxygenated solution due to a partial quenching of the low energy phosphorescent band (Figure 9a, blue line). The determined phosphorescence quantum yield in degassed solution is 17% and is reduced to 2% in air equilibrated solution. The excitation spectra of both bands correlate with the absorption spectrum in the low energy region, indicating that both emissions came from the same complex. However, the excitation spectra are not exactly identical in the region around

https://doi.org/10.1021/acs.inorgchem.3c03532
Inorg. Chem. 2024, 63, 1589−1606

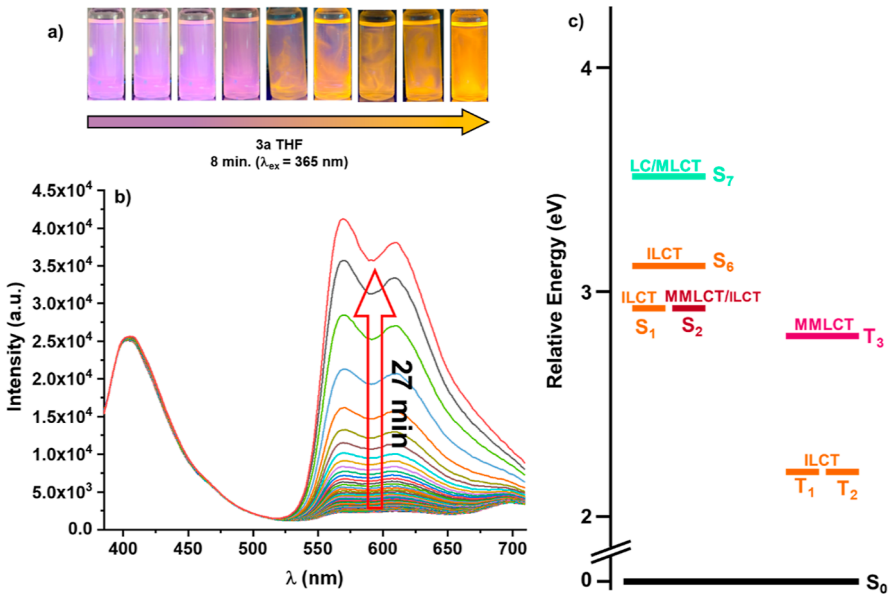

Figure 10. (a) Photographs showing the *switch-on* and enhancement of the phosphorescent emission of **3a** in an aerated THF solution upon excitation at 365 nm. (b) Emission spectra of **3a** in THF 5×10^{-4} M solution in the presence of O_2 with different irradiation times. (c) Relative energy and character of the more intense vertical singlet and triplet excitations at the S_0 geometry of **3a**.

365−400 nm, where there is a notable MLCT contribution. This suggests that, while the fluorescent HE band mainly proceeds of excitation of the ^{1}ILCT, the phosphorescent LE band is also notably populated from high-energy S_n excited states. Interestingly, we also observe that the emission depends on the excitation wavelength. Thus, upon excitation at 365 nm, a dual emission is also observed formed by a short-lived blue-shifted fluorescence band (1.6 ns) located at 405 nm and the structured low energy phosphorescent at 570 nm, which is extremely air sensitive being nearly absent in air-equilibrated THF solution (decreases from 23% in degassed solution to less of 1% in air equilibrated). The new fluorescence band is related to an excitation manifold located at 350 nm, whereas the excitation spectrum when detected the LE band is identical to that observed for the LE band upon exciting in the low energy region (400−450 nm) (Figure 9b). Our calculations suggest that the excitation S_7, at 351.3 nm, has mixed ^{1}MLCT/^{1}LC nature with a remarkable platinum contribution and minor contribution of the NMe_2 (Figure 10b). In agreement with this, the high quantum efficiency in **3a** upon excitation to 365 nm (ϕ = 23%) is mainly attributable to its higher k_r (2.6×10^4) and lesser k_{nr} (8.9×10^4) in relation to those obtained upon excitation to 400−450 nm (Table 2), probably related to the higher metal contribution in the LE emission using the high-energy excitation wavelengths. This wavelength dependence suggests the occurrence of hyper-intersystem crossing (HISC) from S_7 (^{1}MLCT/^{1}LC) to T_1, i.e., relaxation from S_7 to T_1 clearly competes with internal conversion (IC) to S_1. It seems that the energy transfer from relaxed (^{1}MLCT/^{1}LC)* to ^{1}ILCT* is nonefficient. This relatively rare behavior has been previously observed in some platinum complexes, being related to the presence of relaxed S_1 states having strong $\pi\pi^*$ characters with an essentially null metal contribution.[17d,32] At 77 K, the fluorescence is lost and only the phosphorescence emission band at 565 nm is developed regardless of the wavelength used in the excitation.

Interestingly, we observed that in aerated THF solution, upon prolonged photoexcitation at 365 nm, a continuous enhancement of the phosphorescent band is observed, rising its maximum intensity in *ca* 27 min (Figure 10b). The process is also visible with a hand UV−vis lamp in which the initial violet emission, attributed to ^{1}MLCT/^{1}LC fluorescence, was gradually changing to a final orange enhanced emission (Figure 10a). The intense orange emission was switched off by simply shaking the solution allowing its oxygenation. A similar process, which is reversible and can be repeated several times, was also observed in DMSO but does not take place in other solvents, such as acetonitrile, toluene, or MeOH. This relatively rare behavior has been previously observed for us[17d] and other groups,[33] being explained by the occurrence of a local sensitization caused by energy transfer from the low energy triplet to $^3O_2$ producing singlet $^1O_2$ able to selectively react with the solvent (THF[34] or DMSO[17d]), thus creating a free oxygen microenvironment that *switch-on* the phosphorescence (^{3}ILCT). The strong sensibility of the phosphorescent emission in this complex (see Table 2) encourages us to determine its efficiency as an $^1O_2$ sensitizer. The singlet oxygen generation of complex **3a** was examined in acetonitrile solution (5×10^{-4} M) on the infrared region detecting the characteristic emission profile of $^1O_2$ at $\lambda_{em} \sim 1274$ nm (Figure S21) upon excitation at both 365 and 400 nm, respectively. Phenalenone (PN), a universal reference compound which can be used in various solvents,[35] has been employed. The measured quantum yield (ϕ_Δ) of $^1O_2$ was notably higher upon exciting at 365 nm than upon exciting at 400 nm (37% vs 11%), in agreement with the higher ^{3}ILCT phosphorescence efficiency (23% vs 17%, Table 2). These values indicate that this complex can be used as a photosensitizer.

In the solid state, this complex (**3a**) displays a broader emission red-shifted at low temperatures (Figure S19), indicating some additional ^{3}MMLCT contribution.

Because the initial structural report of a diplatinum d^7−d^7 complex, $K_2[Pt_2(SO_4)_4(H_2O)_2]$,[36] different types of high-valent diplatinum d^7−d^7, either with bridging and unbridged ligands, have been reported.[37] These complexes have attracted a great interest in many efficient catalyst processes, such as the

https://doi.org/10.1021/acs.inorgchem.3c03532
Inorg. Chem. 2024, 63, 1589−1606

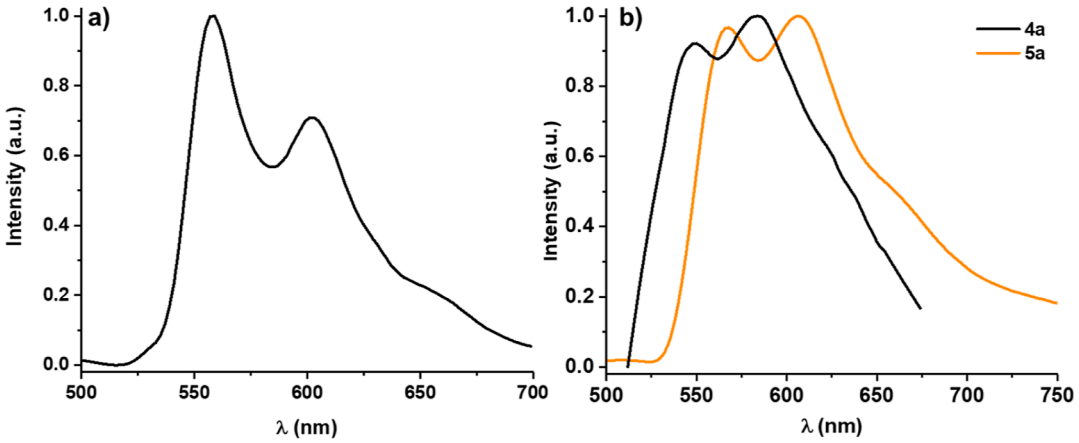

Figure 11. Emission spectra (λ_{ex} 365−420 nm) of (a) **4a** in THF solution (5×10^{-5} M) at 77 K and (b) of **4a** and **5a** in the PS film (10% wt).

oxidation of unsaturated organic molecules, facilitated by the strong electron-withdrawing ability of the unusually high oxidation state of the Pt^{III} atom.[37a] Initial suggestions[38] and recent contributions[13,39] support that these complexes can be sometimes key intermediate in the oxidation pathway from Pt^{II} to Pt^{IV}. Indeed, their rich reactivity indicates that the electron distribution along the Pt−Pt bond can be viewed as a resonance structure between Pt^{III}−Pt^{III} and Pt^{II}−Pt^{IV}.[37e,40] Despite their rich chemistry, and also the well-known emissive properties of either Pt^{II} and Pt^{IV} complexes, reports on emissive d^7−d^7 derivatives are quite rare, mainly due to the fact that in these complexes the target orbital and therefore, the lowest-lying excited state possess metal−metal antibonding ($d\sigma^*_{M\text{-}M}$) character,[28] being therefore short life and nonemissive. To the best of our knowledge, only three types of luminescent binuclear Pt^{III} complexes have been reported: (i) of the type $[Pt_2(\mu\text{-pop})_4X_2]^{4-}$ (pop = P,P-pyrophosphite, $P_2O_5H_2^{2-}$; X = Cl, Br, SCN) or $[Pt_2(\mu\text{-pop})_4X_2]^{2-}$ (X = py);[41] (ii) type $[Pt_2(\mu\text{-}C_6H_3\text{-}5R\text{-}2\text{-}AsPh_2)_4X_2]$ (R = methyl o isopropyl, X = Cl, Br, I)[14a] and (iii) $[Pt(C^N)(\mu\text{-pxdt})]_2$ (pxdt = oxadiazole-thiol). In these latter, donor−acceptor bridging ligands have been employed giving rise to emission from an excited state having ligand-to-metal−metal charge transfer-(LMMCT) character.[14b]

The Pt^{III}−Pt^{III} complexes (**4a** and **5a**) are weakly emissive, showing in PS rigid media and in glassy THF solution (only **4a**), a structured low-efficient (2% **4a** and <1% **5a** in PS) emission profile associated with a ^{3}IL character centered on the R-pbt group (550 **4a** and 566 nm **5a**) (Figure 11). The lowest TD-DFT ($T_{1,2}$ for **4a** and T_{1-3} for **5a**) vertical excitations at the S_0 geometry (Table S4) are of LMMCT/LXCT in nature and are expected to be not emissive, in accordance with the lack of emission in fluid solution. The weak emission observed in rigid media is tentatively associated with close higher excited states (T_3 for **4a** and T_4 for **5a**) having a mainly ^{3}ILCT character with a minor ^{3}MLCT/^{3}XLCT additional contribution for **4** (see Table S4). The calculated values (487.5 nm **4a** and 603 nm **5a**) agree with the experimental red shift observed for **5a** relative to **4a** attributed to the incorporation of the donor NMe_2 group, which increases the energy of the HOMO decreasing the gap of the transition.

Electrochemical Properties. The electrochemical properties of complexes **2a**−**5a** were investigated using cyclic voltammetry in anhydrous CH_2Cl_2 with $(NBu_4)PF_6$ as a supporting electrolyte in the dark.

The potentials and HOMO/LUMO energy estimations are listed in Table 3 and voltammograms covering the anodic (**2a**, **3a**) and cathodic (**2a**−**5a**) regions are depicted in Figure S22. Cyclometalated diplatinum complexes with butterfly or half-lantern shape exhibit mainly a two-electron oxidation process, assignable to the oxidation of the divalent species Pt_2(II) to trivalent species Pt_2(III);[8b,d,12,42] although in some cases, two one-electron redox waves corresponding to the Pt_2(III)/Pt_2(II) couple were observed.[43] The Pt^{II}−Pt^{II} complexes **2a** and **3a** show in the anionic window two bad resolved quasi-reversible or irreversible process with E^{ox} 0.63, 0.96 V **2a**, 0.73, and 1.07 V **3a** (vs Ag/AgCl), probably due to two steps of one-electron oxidation from Pt_2(II,II) to Pt_2(III,II) and to Pt_2(III,III). The irreversibility of the oxidation processes is caused by the nucleophilic reactions of the coordinating solvent to the electrogenerated Pt^{III} species.[12] The Pt^{III}−Pt^{III} complexes **4a** and **5a** do not exhibit significant redox peaks by scanning the potential in the anodic direction.

Complexes constructed with the NMe_2-pbt cyclometalating ligand show an irreversible reduction wave with shape and potential values that are similar (E^{red} −1.10 V Pt_2^{II} **3a**, −1.07 V Pt_2^{III} **5a**). However, the pbt complexes displays different reduction behavior. Thus, whereas the Pt_2^{II} complex **2a** shows an irreversible wave at −1.01 V, two reduction waves at −0.69 and −1.21 V were resolved for **4a** (Pt_2^{III}). HOMO and LUMO

Table 3. Electrochemical Data[a] and HOMO/LUMO Energy Estimations for Complexes 2a−5a

	cyclic voltammetry				DFT calculations	
	E^{ox}[b] (V)	E^{red}[c] (V)	E_{HOMO}[d] (eV)	E_{LUMO}[d] (eV)	E_{HOMO}[e] (eV)	E_{LUMO}[e] (eV)
2a	0.63 0.96	−1.01	−4.98	−3.35	−5.46	−2.00
3a	0.73 1.07	−1.10	−5.07	−3.24	−5.06	−1.67
4a		−0.69 −1.21		−3.13	−6.28	−2.97
5a		−1.07		−3.27	−5.12	−2.84

[a]All measurements were carried out in dark conditions at 298 K in 0.1 M solution of $(NBu_4)PF_6$ in dry CH_2Cl_2 at 100 mV s^{-1} vs Ag/AgCl reference electrode. [b]Quasi-reversible or irreversible anodic peaks. [c]Irreversible cathodic peaks. [d]Estimated HOMO/LUMO energy by electrochemistry data [$E_{HOMO/LUMO} = -(E^{ox/red} + 4.8 - E^{Fc/Fc+})$]. [e]Estimated HOMO/LUMO energy by DFT calculations.

https://doi.org/10.1021/acs.inorgchem.3c03532
Inorg. Chem. 2024, 63, 1589−1606

energy levels were estimated from these CV data by using the relationship $E_{HOMO/LUMO} = -(E^{ox/red} + 4.8 - E^{Fc/Fc+})$, where $E^{Fc/Fc+}$ (0.45 V) is the potential of ferrocene vs Ag/AgCl and 4.8 eV is the energy level of ferrocene to the vacuum energy level. The calculated LUMO energies are between −3.13 and −3.35 V, being similar for the NMe_2-pbt complexes (−3.24 **3a**, −3.27 V **5a**), what is an accordance with a LUMO mainly located in the cyclometalated ligand. Notwithstanding, the estimated HOMO and LUMO energies do not correlate well with those obtained by DFT calculations.

Photocatalytic Studies. In recent years, visible light photocatalysis has received a great attention allowing to furnish new molecules and structural motifs with lower energy consuming when compared with reactions under thermal or ultraviolet (UV).[44] In this area, luminescent cyclometalated transition metals (Ru^{II}, Ir^{III} and Pt^{II}) are among the most frequently employed sensitizers for energy transfer and photoredox catalysis.[45] In particular, some of these complexes have been previously described as efficient photosensitizers for the generation of reactive oxygen species ($^1O_2$, $O_2^{\bullet-}$), being successfully employed as photocatalysts for the photooxidation of different organic molecules.[46] Among the various oxidation reactions, the photo generation of sulfoxides from sulfides using oxygen as oxidant is of great interest,[21,23a,c,47] mainly due to its relevance in the synthesis of biologically active compounds used in the pharmaceutical industry and also in organic synthesis.[18] We recently reported the ability of dimethylphenylbenzothiazole platinum complexes to generate, under photoexcitation, sensitized singlet oxygen ($^1O_2$) able to induce oxidation of DMSO to $DMSO_2$.[17d] In this line, the good ability of complex **3a** to photo sensitize singlet oxygen encouraged us to estimate its photocatalytic activity. In particular, we investigated the induced photooxidation ability of *p*-bromothioanisole (Scheme 4) under

Scheme 4. Photooxidation of *p*-Bromothioanisole to the Corresponding Sulfoxide[a]

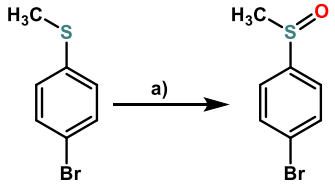

[a]Reagents and conditions: (a) CD_3OD, Blue LED (460 nm), photosensitizer (**3a**).

visible light (blue light; λ = 460 nm) in the presence of **3a** and oxygen as a model for heterogeneous catalysis.[48] The evolution of the catalysis was monitored by NMR spectroscopy. Photosensitizer **3a** showed a good photostability under irradiation of blue light in suspension and solid state (measured by UV−vis spectroscopy from 0 to 50 h, Figure S23). This reaction was evaluated in different conditions and molar ratio of catalyst and substrate (Table 4, entries 1 and 2), with 1 and 5 mol % of the metal complex. In both cases, the reaction occurred with similar results allowing >95% conversion after 50 h of reaction. However, with 5% the reaction shows slight greater efficiencies at shorter times (3−4 h of reaction, Table S11). As illustration, after 15 h of reaction with 1% showed a 45% conversion, while with 5% a 55%. These results allow us to conclude that the increase of the amount of catalyst does not produce remarkable changes in the efficiencies.

Table 4. Heterogeneous Visible-Light Oxidative Reactions with Different Conditions

entry	% photosensitizer (%)	light	atmosphere	time (h)	conversion (%)
1	1	+	air	50	>95
2	5	+	air	50	>95
3[a]	5	+	air	36	>95
4	1	+	N_2	50	−
5	1	−	air	50	−
6	−	+	air	50	−
7[b]	1	+	air	50	10
8[c]	1	+	air	50	23

[a]Double amount of reagent (*p*-bromothioanisole) and photosensitizer than in the entry 2. [b]In the presence of DABCO. [c]In the presence of BQ.

When the reaction was carried out with double amount of catalyst and substrate (Table 4, entry 3), the 95% of conversion was reached at 36 h, revealing that the increment in the concentration of the photocatalytic reactions improves the efficiency. Under hypoxic conditions, the conversion was considerably reduced because of the impossibility to produce ROS in the absence of oxygen (Table 4, entry 4). In the absence of light (Table 4, entry 5), no conversion was observed and, similarly, without a catalyst (**3a**) in the presence of air the reaction does not take place (Table 4, entry 6).

Generally, two mechanisms involving two main ROS intermediates such as $^1O_2$ and $O_2^{\bullet-}$ have been proposed for the photocatalytic oxidation of sulfides:[49] (a) The photooxygenation promoted by $^1O_2$ generated by a photosensitizer and (b) a photosensitized electron-transfer (ET) oxidation using $^3O_2$ through $O_2{}^{*-}$ as an intermediate. In both mechanisms, a similar zwitterionic persulfide intermediate ($R_1R_2S^+O-O^-$) is proposed, which reacts with a second molecule of R_1R_2S leading to the formation of two molecular sulfoxides. Discrimination between both mechanisms is not an easy task.[21] To get insights into the catalytic mechanism, several control experiments were carried out. Thus, the photocatalytic reaction was evaluated out in the presence of 1,4-diazabicyclo[2.2.2]octane (DABCO), a well-known singlet oxygen quencher, to evaluate the potential production of these species. As can be observed in the Table 2-entry 7, in the presence of DABCO (3 equiv), reagents (sulfide, **3a**), and light, the reaction is notably reduced (10%) and only traces of oxidized product were obtained, pointing to a key role of complex **3a** as an oxygen sensitizer. On the other hand, the addition of a superoxide radical ($O_2^{\bullet-}$) quencher like 1,4-benzoquinone (BQ, 3 equiv) to the photooxidation process (Table 4, entry 8) also results in a remarkable decrease of the reaction yield to 23%, revealing a key role of these reactive oxygen species too. These observations suggest that both $^1O_2$ and superoxide radicals play an important role in this photocatalytic reaction.

CONCLUSIONS

In summary, we have prepared novel series of mononuclear (**1a−c**), bimetallic ($Pt^{II}-Pt^{II}$) (**2a−c**, **3a**), and ($Pt^{III}-Pt^{III}$) (**4a**, **5a**) complexes incorporating phenylbenzothiazole (pbt) and 2-(4-dimethylaminophenyl)benzothiazole (Me_2N-pbt) as cyclometalating chromophore groups and pyrazole (**1**) or pyrazolate bridging ligands (**2−5**). Experimental data and computational studies reveal the negligible influence of the pyrazole or

https://doi.org/10.1021/acs.inorgchem.3c03532
Inorg. Chem. 2024, 63, 1589−1606

pyrazolate bridging ligand on the optical properties of complexes **1a−c** and **2a,b**, which exhibit typical low-lying IL/MLCT electronic transitions. Only complex **2c**, incorporating the bulky 3,5-$^{i}Pr_2$pz bridging groups exhibits in the solid state an emission with some contribution of the ^{3}MMLCT excited state, which is clearly predominant at low temperatures (560 nm at 298 K; 600 nm 77 K). **3a** incorporating the donor−acceptor Me_2N-pbt ligand displays unusual dual, Fluorescence (^{1}ILCT or ^{1}MLCT/^{1}LC) and phosphorescence (^{3}ILCT) emissions depending on the excitation wavelength. The efficiency of the population of the triplet manifold increases upon photoexcitation of excited states having a higher metal d contribution. The phosphorescence can be reversibly photoinduced in oxygenated THF and DMSO solutions upon continuous excitation (365 nm, ∼ 15 min) and quenched by shaking. The complex also photosensitizes $^1O_2$, with a higher quantum yield at λ_{ex} of 365 nm than at 400 nm (37 vs 11%). Computed results for the low-lying T_1−T_3 excited states in complexes **2a** and **3a** indicate that $T_{1,2}$ have a mixed ^{3}IL/^{3}MLCT nature in **2a** and mainly ^{3}ILCT character in **3a**. In both complexes, the T_3 has a ^{3}MMLCT character and lies more separated from T_1 (0.6 eV) in **3a** than in **2a** (0.3 eV). The diplatinum complexes **4a** and **5a** increase the small number of luminescent d^7−d^7 compounds reported, with a weak emission, in rigid media, ascribed to ^{3}ILCT. Finally, complex **3a**, which demonstrates the ability to photosensitize singlet oxygen, has been further applied for the photooxidation of *p*-bromothioanisol under visible light (460 nm). Control of this reaction suggests that both, $^1O_2$ and superoxide radicals, play an important role in this photocatalytic reaction.

■ ASSOCIATED CONTENT

Supporting Information

The Supporting Information is available free of charge at https://pubs.acs.org/doi/10.1021/acs.inorgchem.3c03532.

Characterization of complexes (NMR spectra, crystal data), photophysical properties and computational details, and photocatalytic studies (PDF)

Accession Codes

CCDC 2297974−2297979 contain the supplementary crystallographic data for this paper. These data can be obtained free of charge via www.ccdc.cam.ac.uk/data_request/cif, or by emailing data_request@ccdc.cam.ac.uk, or by contacting The Cambridge Crystallographic Data Centre, 12 Union Road, Cambridge CB2 1EZ, UK; fax: +44 1223 336033.

■ AUTHOR INFORMATION

Corresponding Authors

M. Teresa Moreno − *Departamento de Química, Instituto de Investigación en Química (IQUR), Complejo Científico Tecnológico, Universidad de La Rioja, Logroño 26006, Spain;* orcid.org/0000-0002-7744-9805; Email: teresa.moreno@unirioja.es

Elena Lalinde − *Departamento de Química, Instituto de Investigación en Química (IQUR), Complejo Científico Tecnológico, Universidad de La Rioja, Logroño 26006, Spain;* orcid.org/0000-0001-7402-1742; Email: elena.lalinde@unirioja.es

Authors

David Gómez de Segura − *Departamento de Química, Instituto de Investigación en Química (IQUR), Complejo Científico Tecnológico, Universidad de La Rioja, Logroño 26006, Spain*

Andrea Corral-Zorzano − *Departamento de Química, Instituto de Investigación en Química (IQUR), Complejo Científico Tecnológico, Universidad de La Rioja, Logroño 26006, Spain*

Eduardo Alcolea − *Departamento de Química, Instituto de Investigación en Química (IQUR), Complejo Científico Tecnológico, Universidad de La Rioja, Logroño 26006, Spain*

Complete contact information is available at: https://pubs.acs.org/10.1021/acs.inorgchem.3c03532

Notes

The authors declare no competing financial interest.

■ ACKNOWLEDGMENTS

This work was supported by the Spanish Ministerio de Ciencia e Innovación (Project PID2019-109742GB-I00) funded by MCIN/AIE/10.13039/501100011033, the "ERDF A way of making Europe" and the "European Union". D.G.S. is grateful to UR for a PhD grant.

■ REFERENCES

(1) (a) Ulbricht, C.; Beyer, B.; Friebe, C.; Winter, A.; Schubert, U. S. Recent Developments in the Application of Phosphorescent Iridium(III) Complex Systems. *Adv. Mater.* **2009**, *21*, 4418−4441. (b) Kajjam, A. B.; Vaidyanathan, S. Structural Mimics of Phenyl Pyridine (ppy) − Substituted, Phosphorescent Cyclometalated Homo and Heteroleptic Iridium(III) Complexes for Organic Light Emitting Diodes − An Overview. *Chem. Rec.* **2018**, *18*, 293−349. (c) Feng, Z.; Sun, Y.; Yang, X.; Zhou, G. Novel Emission Color-Tuning Strategies in Heteroleptic Phosphorescent Ir(III) and Pt(II) Complexes. *Chem. Rec.* **2019**, *19*, 1710−1728. (d) McConnell, A. J.; Wood, C. S.; Neelakandan, P. P.; Nitschke, J. R. Stimuli-Responsive Metal−Ligand Assemblies. *Chem. Rev.* **2015**, *115*, 7729−7793. (e) Teegardin, K.; Day, J. I.; Chan, J.; Weaver, J. Advances in Photocatalysis: A Microreview of Visible Light Mediated Ruthenium and Iridium Catalyzed Organic Transformations. *Org. Process Res. Dev.* **2016**, *20*, 1156−1163. (f) To, W.-P.; Wan, Q.; Tong, G. S. M.; Che, C.-M. Recent Advances in Metal Triplet Emitters with d^6, d^8, and d^{10} Electronic Configurations. *Trends. Chem.* **2020**, *2*, 796−812. (g) Zhang, X.; Hou, Y.; Xiao, X.; Chen, X.; Hu, M.; Geng, X.; Wang, Z.; Zhao, J. Recent development of the transition metal complexes showing strong absorption of visible light and long-lived triplet excited state: From molecular structure design to photophysical properties and applications. *Coord. Chem. Rev.* **2020**, *417*, 213371. (h) Lee, S.; Han, W.-S. Cyclometalated Ir(III) complexes towards blue-emissive dopant for organic light-emitting diodes: fundamentals of photophysics and designing strategies. *Inorg. Chem. Front.* **2020**, *7*, 2396−2422. (i) Pashaei, B.; Karimi, S.; Shahroosvand, H.; Abbasi, P.; Pilkington, M.; Bartolotta, A.; Fresta, E.; Fernandez-Cestau, J.; Costa, R. D.; Bonaccorso, F. Polypyridyl ligands as a versatile platform for solid-state light-emitting devices. *Chem. Soc. Rev.* **2019**, *48*, 5033−5139. (j) Lin, Y.-D.; Tsai, W.-W.; Lu, C.-W. Exploring the Electroluminescent Applications of Imidazole Derivatives. *Chem.—Eur. J.* **2023**, *29*, No. e202203040. (k) Buil, M. L.; Esteruelas, M. A.; López, A. M. Recent Advances in Synthesis of Molecular Heteroleptic Osmium and Iridium Phosphorescent Emitters. *Eur. J. Inorg. Chem.* **2021**, *2021*, 4731−4761.

(2) (a) Díez, Á.; Lalinde, E.; Moreno, M. T. Heteropolynuclear cycloplatinated complexes: Structural and photophysical properties. *Coord. Chem. Rev.* **2011**, *255*, 2426−2447. (b) Aliprandi, A.; Genovese, D.; Mauro, M.; De Cola, L. Recent Advances in Phosphorescent Pt(II) Complexes Featuring Metallophilic Interactions: Properties and Applications. *Chem. Lett.* **2015**, *44*, 1152−1169. (c) Li, K.; Ming Tong, G. S.; Wan, Q.; Cheng, G.; Tong, W.-Y.; Ang, W.-H.; Kwong, W.-

L.; Che, C.-M. Highly phosphorescent platinum(II) emitters: photophysics, materials and biological applications. *Chem. Sci.* **2016**, *7*, 1653−1673. (d) Cebrián, C.; Mauro, M. Recent advances in phosphorescent platinum complexes for organic light-emitting diodes. *Beilstein J. Org. Chem.* **2018**, *14*, 1459−1481. (e) Puttock, E. V.; Walden, M. T.; Williams, J. G. The luminescence properties of multinuclear platinum complexes. *Coord. Chem. Rev.* **2018**, *367*, 127−162. (f) Berenguer, J. R.; Lalinde, E.; Moreno, M. T. Luminescent cyclometalated-pentafluorophenyl Pt^{II}, Pt^{IV} and heteropolynuclear complexes. *Coord. Chem. Rev.* **2018**, *366*, 69−90. (g) Yam, V. W.-W.; Law, A. S.-Y. Luminescent d^8 metal complexes of platinum(II) and gold(III): From photophysics to photofunctional materials and probes. *Coord. Chem. Rev.* **2020**, *414*, 213298. (h) Yoshida, M.; Kato, M. Cation-controlled luminescence behavior of anionic cyclometalated platinum(II) complexes. *Coord. Chem. Rev.* **2020**, *408*, 213194. (i) Sadeghian, M.; Haghighi, M. G.; Lalinde, E.; Teresa Moreno, M. Group 10 metal-cyanide scaffolds in complexes and extended frameworks: Properties and applications. *Coord. Chem. Rev.* **2022**, *452*, 214310.

(3) Chen, Z.; Ho, C.-L.; Wang, L.; Wong, W.-Y. Single-Molecular White-Light Emitters and Their Potential WOLED Applications. *Adv. Mater.* **2020**, *32*, 1903269.

(4) (a) Chen, Z.; Chan, M. H.-Y.; Yam, V. W.-W. Stimuli-Responsive Two-Dimensional Supramolecular Polymers Based on Trinuclear Platinum(II) Scaffolds: Reversible Modulation of Photoluminescence, Cavity Size, and Water Permeability. *J. Am. Chem. Soc.* **2020**, *142*, 16471−16478. (b) Ai, Y.; Li, Y.; Chan, M. H.-Y.; Xiao, G.; Zou, B.; Yam, V. W.-W. Realization of Distinct Mechano- and Piezochromic Behaviors via Alkoxy Chain Length-Modulated Phosphorescent Properties and Multidimensional Self-Assembly Structures of Dinuclear Platinum(II) Complexes. *J. Am. Chem. Soc.* **2021**, *143*, 10659−10667. (c) Martínez-Junquera, M.; Lalinde, E.; Moreno, M. T. Multistimuli-Responsive Properties of Aggregated Isocyanide Cycloplatinated(II) Complexes. *Inorg. Chem.* **2022**, *61*, 10898−10914. (d) Gómez de Segura, D.; Lalinde, E.; Moreno, M. T. Polymorphism and Mechanochromism in 2-Phenylbenzothiazole Cyclometalated Pt^{II} Complexes with Chelating N^O Ligands. *Inorg. Chem.* **2022**, *61*, 20043−20056. (e) Bryant, M. J.; Skelton, J. M.; Hatcher, L. E.; Stubbs, C.; Madrid, E.; Pallipurath, A. R.; Thomas, L. H.; Woodall, C. H.; Christensen, J.; Fuertes, S.; Robinson, T. P.; Beavers, C. M.; Teat, S. J.; Warren, M. R.; Pradaux-Caggiano, F.; Walsh, A.; Marken, F.; Carbery, D. R.; Parker, S. C.; McKeown, N. B.; Malpass-Evans, R.; Carta, M.; Raithby, P. R. A rapidly-reversible absorptive and emissive vapochromic Pt(II) pincer-based chemical sensor. *Nat. Commun.* **2017**, *8*, 1800.

(5) (a) Tuong Ly, K.; Chen-Cheng, R.-W.; Lin, H.-W.; Shiau, Y.-J.; Liu, S.-H.; Chou, P.-T.; Tsao, C.-S.; Huang, Y.-C.; Chi, Y. Near-infrared organic light-emitting diodes with very high external quantum efficiency and radiance. *Nat. Photonics* **2017**, *11*, 63−68. (b) Zhang, Y.; Wang, Y.; Song, J.; Qu, J.; Li, B.; Zhu, W.; Wong, W.-Y. Near-Infrared Emitting Materials via Harvesting Triplet Excitons: Molecular Design, Properties, and Application in Organic Light Emitting Diodes. *Adv. Opt. Mater.* **2018**, *6*, 1800466. (c) Yang, X.; Guo, H.; Xu, X.; Sun, Y.; Zhou, G.; Ma, W.; Wu, Z. Enhancing Molecular Aggregations by Intermolecular Hydrogen Bonds to Develop Phosphorescent Emitters for High-Performance Near-Infrared OLEDs. *Adv. Sci.* **2019**, *6*, 1801930. (d) Wang, L.; Miao, J.; Zhang, Y.; Wu, C.; Huang, H.; Wang, X.; Yang, C. Discrete Mononuclear Platinum(II) Complexes Realize High-Performance Red Phosphorescent OLEDs with EQEs of up to 31.8% and Superb Device Stability. *Adv. Mater.* **2023**, *35*, 2303066.

(6) Law, A. S.-Y.; Lee, L. C.-C.; Lo, K. K.-W.; Yam, V. W.-W. Aggregation and Supramolecular Self-Assembly of Low-Energy Red Luminescent Alkynylplatinum(II) Complexes for RNA Detection, Nucleolus Imaging, and RNA Synthesis Inhibitor Screening. *J. Am. Chem. Soc.* **2021**, *143*, 5396−5405.

(7) (a) Sun, Y.; Liu, B.; Guo, Y.; Chen, X.; Lee, Y.-T.; Feng, Z.; Adachi, C.; Zhou, G.; Chen, Z.; Yang, X. Developing Efficient Dinuclear Pt(II) Complexes Based on the Triphenylamine Core for High-Efficiency Solution-Processed OLEDs. *ACS Appl. Mater. Interfaces* **2021**, *13*, 36020−36032. (b) Culham, S.; Lanoë, P. H.; Whittle, V. L.; Durrant, M. C.; Williams, J. A. G.; Kozhevnikov, V. N. Highly Luminescent Dinuclear Platinum(II) Complexes Incorporating Bis-Cyclometallating Pyrazine-Based Ligands: A Versatile Approach to Efficient Red Phosphors. *Inorg. Chem.* **2013**, *52*, 10992−11003. (c) Shafikov, M. Z.; Daniels, R.; Pander, P.; Dias, F. B.; Williams, J. A. G.; Kozhevnikov, V. N. Dinuclear Design of a Pt(II) Complex Affording Highly Efficient Red Emission: Photophysical Properties and Application in Solution-Processible OLEDs. *ACS Appl. Mater. Interfaces* **2019**, *11*, 8182−8193.

(8) (a) Chaaban, M.; Zhou, C.; Lin, H.; Chyi, B.; Ma, B. Platinum(II) binuclear complexes: molecular structures, photophysical properties, and applications. *J. Mater. Chem. C* **2019**, *7*, 5910−5924. (b) Katlenok, E. A.; Kryukov, D. M.; Kurtsevich, A. E.; Degtyarenko, K. M.; Valiev, R. R.; Levin, O. V.; Kukushkin, V. Y.; Rozhkov, A. V. Incorporation of a Fluorine Atom in a Bridging Ligand of Half-Lantern Pt_2^{II} Complexes Provides up to 10-Fold Enhancement of Electroluminescence Brightness. *Inorg. Chem.* **2023**, *62*, 11080−11094. (c) Park, H. J.; Boelke, C. L.; Cheong, P. H.-Y.; Hwang, D.-H. Dinuclear Pt(II) Complexes with Red and NIR Emission Governed by Ligand Control of the Intramolecular Pt−Pt Distance. *Inorg. Chem.* **2022**, *61*, 5178−5183. (d) Roy, S.; Lopez, A. A.; Yarnell, J. E.; Castellano, F. N. Metal−Metal-to-Ligand Charge Transfer in Pt(II) Dimers Bridged by Pyridyl and Quinoline Thiols. *Inorg. Chem.* **2022**, *61*, 121−130.

(9) (a) Leshchev, D. J. S.; J S Valentine, A.; Kim, P.; Mills, A. W.; Roy, S.; Chakraborty, A.; Biasin, E.; Haldrup, K.; Hsu, D. J.; Kirschner, M. S.; Rimmerman, D.; Chollet, M.; Glownia, J. M.; van Driel, T. B.; Castellano, F. N.; Li, X.; Chen, L. X. Revealing Excited-State Trajectories on Potential Energy Surfaces with Atomic Resolution in Real Time. *Angew. Chem., Int. Ed.* **2023**, *62*, No. e202304615. (b) Kim, P.; Valentine, A. J. S.; Roy, S.; Mills, A. W.; Chakraborty, A.; Castellano, F. N.; Li, X.; Chen, L. X. Ultrafast Excited-State Dynamics of Photoluminescent Pt(II) Dimers Probed by a Coherent Vibrational Wavepacket. *J. Phys. Chem.Lett.* **2021**, *12*, 6794−6803.

(10) (a) Horiuchi, S.; Umakoshi, K. Recent advances in pyrazolato-bridged homo- and heterometallic polynuclear platinum and palladium complexes. *Coord. Chem. Rev.* **2023**, *476*, 214924. (b) Sicilia, V.; Arnal, L.; Fuertes, S.; Martín, A.; Baya, M. Metal−Metal Cooperation in the Oxidation of a Flapping Platinum Butterfly by Haloforms: Experimental and Theoretical Evidence. *Inorg. Chem.* **2020**, *59*, 12586−12594.

(11) (a) Mewes, L.; Ingle, R. A.; Megow, S.; Böhnke, H.; Baranoff, E.; Temps, F.; Chergui, M. Ultrafast Intersystem Crossing and Structural Dynamics of $[Pt(ppy)(\mu\text{-}^tBu_2pz)]_2$. *Inorg. Chem.* **2020**, *59*, 14643−14653. (b) Luo, Y.; Cheng, Y.; Zhang, D.; Mei, X.; Tang, D.; Hu, J.; Luo, T. Controlling the Triplet Potential Energy Surface of Bimetallic Platinum(II) Complex by Constructing Structure−Property Relationship: A Theoretical Exploration. *Inorg. Chem.* **2023**, *62*, 2440−2455.

(12) Chakraborty, A.; Deaton, J. C.; Haefele, A.; Castellano, F. N. Charge-Transfer and Ligand-Localized Photophysics in Luminescent Cyclometalated Pyrazolate-Bridged Dinuclear Platinum(II) Complexes. *Organometallics* **2013**, *32*, 3819−3829.

(13) Soto, M. A.; Chaudhry, M. T.; Matharu, G. K.; Lelj, F.; MacLachlan, M. J. Molecular Flytraps Held Together by Platinum−Platinum Intermetallic Bonds. *Angew. Chem., Int. Ed.* **2023**, *62*, No. e202305525.

(14) (a) Bennett, M. A.; Bhargava, S. K.; Cheng, E. C.-C.; Lam, W. H.; Lee, T. K.-M.; Privér, S. H.; Wagler, J.; Willis, A. C.; Yam, V. W.-W. Unprecedented Near-Infrared (NIR) Emission in Diplatinum(III) (d^7−d^7) Complexes at Room Temperature. *J. Am. Chem. Soc.* **2010**, *132*, 7094−7103. (b) Wu, X.; Chen, D.-G.; Liu, D.; Liu, S.-H.; Shen, S.-W.; Wu, C.-I.; Xie, G.; Zhou, J.; Huang, Z.-X.; Huang, C.-Y.; Su, S.-J.; Zhu, W.; Chou, P.-T. Highly Emissive Dinuclear Platinum(III) Complexes. *J. Am. Chem. Soc.* **2020**, *142*, 7469−7479.

(15) (a) Hroch, L.; Aitken, L.; Benek, O.; Dolezal, M.; Kuca, K.; Gunn-Moore, F.; Musilek, K. Benzothiazoles - Scaffold of Interest for CNS Targeted Drugs. *Curr. Med. Chem.* **2015**, *22*, 730−747. (b) Feng, G.; Luo, X.; Lu, X.; Xie, S.; Deng, L.; Kang, W.; He, F.; Zhang, J.; Lei, C.; Lin, B.; Huang, Y.; Nie, Z.; Yao, S. Engineering of Nucleic Acids and Synthetic Cofactors as Holo Sensors for Probing Signaling Molecules in

https://doi.org/10.1021/acs.inorgchem.3c03532
Inorg. Chem. 2024, 63, 1589−1606

the Cellular Membrane Microenvironment. *Angew. Chem., Int. Ed.* **2019**, *58*, 6590−6594. (c) Ammazzalorso, A.; Carradori, S.; Amoroso, R.; Fernández, I. F. 2-substituted benzothiazoles as antiproliferative agents: Novel insights on structure-activity relationships. *Eur. J. Med. Chem.* **2020**, *207*, 112762.

(16) (a) Chen, S.-H.; Jiang, K.; Lin, J.-Y.; Yang, K.; Cao, X.-Y.; Luo, X.-Y.; Wang, Z.-Y. Rational design and synthesis of Y-shaped fluorophores with multifarious emission properties and their application in the sensitive detection of PA. *J. Mater. Chem. C* **2020**, *8*, 8257−8267. (b) Thekkeppat, N. P.; Lakshmipathi, M.; Jalilov, A. S.; Das, P.; Peedikakkal, A. M. P.; Ghosh, S. Combining Optical Properties with Flexibility in Halogen-Substituted Benzothiazole Crystals. *Cryst. Growth Des.* **2020**, *20*, 3937−3943.

(17) (a) Lara, R.; Lalinde, E.; Moreno, M. T. Phosphorescent platinum(II) alkynyls end-capped with benzothiazole units. *Dalton Trans.* **2017**, *46*, 4628−4641. (b) Lalinde, E.; Lara, R.; López, I. P.; Moreno, M. T.; Alfaro-Arnedo, E.; Pichel, J. G.; Piñeiro-Hermida, S. Benzothiazole-Based Cycloplatinated Chromophores: Synthetic, Optical, and Biological Studies. *Chem.—Eur. J.* **2018**, *24*, 2440−2456. (c) Giménez, N.; Lalinde, E.; Lara, R.; Moreno, M. T. Design of Luminescent, Heteroleptic, Cyclometalated Pt^{II} and Pt^{IV} Complexes: Photophysics and Effects of the Cyclometalated Ligands. *Chem.—Eur. J.* **2019**, *25*, 5514−5526. (d) Lara, R.; Millán, G.; Moreno, M. T.; Lalinde, E.; Alfaro-Arnedo, E.; López, I. P.; Larráyoz, I. M.; Pichel, J. G. Investigation on Optical and Biological Properties of 2-(4-Dimethylaminophenyl)benzothiazole Based Cycloplatinated Complexes. *Chem.—Eur. J.* **2021**, *27*, 15757−15772. (e) Gómez de Segura, D.; Lara, R.; Martínez-Junquera, M.; Lalinde, E.; Moreno, M. T. Luminescent 2-phenylbenzothiazole cyclometalated Pt^{II} and Ir^{III} complexes with chelating P^O ligands. *Dalton Trans.* **2022**, *51*, 274−285. (f) Millán, G.; Nieddu, M.; López, I. P.; Ezquerro, C.; Berenguer, J. R.; Larráyoz, I. M.; Pichel, J. G.; Lalinde, E. A new family of luminescent iridium complexes: synthesis, optical, and cytotoxic studies. *Dalton Trans.* **2023**, *52*, 6360−6374. (g) Corral-Zorzano, A.; Gómez de Segura, D.; Lalinde, E.; Moreno, M. T. Phosphorescent 2-phenylbenzothiazole Pt^{IV} bis-cyclometalated complexes with phenanthroline-based ligands. *Dalton Trans.* **2023**, *52*, 6543−6550.

(18) (a) Legros, J.; Dehli, J. R.; Bolm, C. Applications of Catalytic Asymmetric Sulfide Oxidations to the Syntheses of Biologically Active Sulfoxides. *Adv. Synth. Catal.* **2005**, *347*, 19−31. (b) Caron, S.; Dugger, R. W.; Ruggeri, S. G.; Ragan, J. A.; Ripin, D. H. Large-Scale Oxidations in the Pharmaceutical Industry. *Chem. Rev.* **2006**, *106*, 2943−2989.

(19) Sipos, G.; Drinkel, E. E.; Dorta, R. The emergence of sulfoxides as efficient ligands in transition metal catalysis. *Chem. Soc. Rev.* **2015**, *44*, 3834−3860.

(20) Gu, X.; Li, X.; Chai, Y.; Yang, Q.; Li, P.; Yao, Y. A simple metal-free catalytic sulfoxidation under visible light and air. *Green Chem.* **2013**, *15*, 357.

(21) Neveselý, T.; Svobodová, E.; Chudoba, J.; Sikorski, M.; Cibulka, R. Efficient Metal-Free Aerobic Photooxidation of Sulfides to Sulfoxides Mediated by a Vitamin B2 Derivative and Visible Light. *Adv. Synth. Catal.* **2016**, *358*, 1654−1663.

(22) Li, W.; Xie, Z.; Jing, X. BODIPY photocatalyzed oxidation of thioanisole under visible light. *Catal. Commun.* **2011**, *16*, 94−97.

(23) (a) Li, L.-P.; Ye, B.-H. Efficient Generation of Singlet Oxygen and Photooxidation of Sulfide into Sulfoxide via Tuning the Ancillary of Bicyclometalated Iridium(III) Complexes. *Inorg. Chem.* **2019**, *58*, 7775−7784. (b) Morozkov, G. V.; Abel, A. S.; Filatov, M. A.; Nefedov, S. E.; Roznyatovsky, V. A.; Cheprakov, A. V.; Mitrofanov, A. Y.; Ziankou, I. S.; Averin, A. D.; Beletskaya, I. P.; Michalak, J.; Bucher, C.; Bonneviot, L.; Bessmertnykh-Lemeune, A. Ruthenium(II) complexes with phosphonate-substituted phenanthroline ligands: synthesis, characterization and use in organic photocatalysis. *Dalton Trans.* **2022**, *51*, 13612−13630. (c) Popov, S.; Plenio, H. Ligand Exchange Triggered Photosensitizers − Bodipy-Tagged NHC-Metal Complexes for Conversion of $^3O_2$ to $^1O_2$. *Eur. J. Inorg. Chem.* **2022**, *2022*, No. e202200335.

(24) Berenguer, J. R.; Pichel, J. G.; Giménez, N.; Lalinde, E.; Moreno, M. T.; Piñeiro-Hermida, S. Luminescent pentafluorophenyl-cyclo-platinated complexes: synthesis, characterization, photophysics, cytotoxicity and cellular imaging. *Dalton Trans.* **2015**, *44*, 18839−18855.

(25) Haque, A.; Alenezi, K. M.; Khan, M. S.; Wong, W.-Y.; Raithby, P. R. Non-covalent interactions (NCIs) in π-conjugated functional materials: advances and perspectives. *Chem. Soc. Rev.* **2023**, *52*, 454−472.

(26) (a) Sakai, K.; Sato, T.; Tsubomura, T.; Matsumoto, K. Di-(μ-pyrazolato-N:N')-bis[(2,2'-bipyridine-N,N')platinum(II)] Bis-(tetrafluoroborate) Monohydrate. *Acta Crystallogr. Sect. C* **1996**, *52*, 783−786. (b) Umakoshi, K.; Kimura, K.; Kim, Y. H.; Tsukimoto, Y.; Arikawa, Y.; Onishi, M.; Ishizaka, S.; Kitamura, N. Pyrazolato- and 3,5-Dimethylpyrazolato-Bridged Dinuclear Platinum(II), Palladium(II), and Their Mixed-Metal Complexes of 2,2′-Bipyrimidine. Syntheses, Structures, and Luminescent Properties. *Bull. Chem. Soc. Jpn.* **2010**, *83*, 1504−1510. (c) Ghavale, N.; Wadawale, A.; Dey, S.; Jain, V. K. Synthesis, structures and spectroscopic properties of platinum complexes containing orthometalated 2-phenylpyridine. *J. Organomet. Chem.* **2010**, *695*, 1237−1245. (d) Ma, B.; Li, J.; Djurovich, P. I.; Yousufuddin, M.; Bau, R.; Thompson, M. E. Synthetic Control of Pt···Pt Separation and Photophysics of Binuclear Platinum Complexes. *J. Am. Chem. Soc.* **2005**, *127*, 28−29. (e) Ma, B.; Djurovich, P. I.; Garon, S.; Alleyne, B.; Thompson, M. E. Platinum Binuclear Complexes as Phosphorescent Dopants for Monochromatic and White Organic Light-Emitting Diodes. *Adv. Funct. Mater.* **2006**, *16*, 2438−2446. (f) Pinter, P.; Soellner, J.; Strassner, T. Photophysical Properties of Phosphorescent Mono- and Bimetallic Platinum(II) Complexes with C^C* Cyclometalating NHC Ligands. *Organometallics* **2021**, *40*, 557−563. (g) Arnal, L.; Escudero, D.; Fuertes, S.; Martin, A.; Sicilia, V. High-Valent Pyrazolate-Bridged Platinum Complexes: A Joint Experimental and Theoretical Study. *Inorg. Chem.* **2022**, *61*, 12559−12569. (h) Arnal, L.; Fuertes, S.; Martín, A.; Baya, M.; Sicilia, V. A Cyclometalated N-Heterocyclic Carbene: The Wings of the First Pt_2 (II,II) Butterfly Oxidized by CHI_3. *Chem.—Eur. J.* **2018**, *24*, 18743−18748. (i) Berenguer, J. R.; Díez, A.; Lalinde, E.; Moreno, M. T.; Ruiz, S.; Sánchez, S. Luminescent Cycloplatinated Complexes Containing Poly (pyrazolyl)-borate and-methane Ligands. *Organometallics* **2011**, *30*, 5776−5792. (j) Leopold, H.; Tenne, M.; Tronnier, A.; Metz, S.; Münster, I.; Wagenblast, G.; Strassner, T. Binuclear C^C* Cyclometalated Platinum(II) NHC Complexes with Bridging Amidinate Ligands. *Angew. Chem., Int. Ed.* **2016**, *55*, 15779−15782. (k) Lo, K.-W.; Tong, G. S. M.; Cheng, G.; Low, K.-H.; Che, C.-M. Dinuclear Pt^{II} Complexes with Strong Blue Phosphorescence for Operationally Stable Organic Light-Emitting Diodes with EQE up to 23% at 1000 cd m^{-2}. *Angew. Chem., Int. Ed.* **2022**, *61*, No. e202115515.

(27) Kim, P.; Kelley, M. S.; Chakraborty, A.; Wong, N. L.; Van Duyne, R. P.; Schatz, G. C.; Castellano, F. N.; Chen, L. X. Coherent Vibrational Wavepacket Dynamics in Platinum(II) Dimers and Their Implications. *J. Phys. Chem. C* **2018**, *122*, 14195−14204.

(28) Sicilia, V.; Baya, M.; Borja, P.; Martín, A. Oxidation of Half-Lantern Pt_2 (II,II) Compounds by Halocarbons. Evidence of Dioxygen Insertion into a Pt(III)−CH_3 Bond. *Inorg. Chem.* **2015**, *54*, 7316−7324.

(29) Zhang, H.; Liu, C.; Yin, G.; Du, C.; Zhang, B. Efficiently luminescent heteroleptic neutral platinum(ii) complexes based on N^O and N^P benzimidazole ligands. *Dalton Trans.* **2021**, *50*, 17319−17327.

(30) Mullin, W. J.; Qin, H.; Mani, T.; Müller, P.; Panzer, M. J.; Thomas, S. W. Turning on solid-state phosphorescence of platinum acetylides with aromatic stacking. *Chem. Commun.* **2020**, *56*, 6854−6857.

(31) (a) Chang, S.-Y.; Chen, J.-L.; Chi, Y.; Cheng, Y.-M.; Lee, G.-H.; Jiang, C.-M.; Chou, P.-T. Blue-Emitting Platinum(II) Complexes Bearing both Pyridylpyrazolate Chelate and Bridging Pyrazolate Ligands: Synthesis, Structures, and Photophysical Properties. *Inorg. Chem.* **2007**, *46*, 11202−11212. (b) Arnal, L.; Fuertes, S.; Martín, A.; Sicilia, V. The Use of Cyclometalated NHCs and Pyrazoles for the Development of Fully Efficient Blue PtII Emitters and Pt/Ag Clusters. *Chem.—Eur. J.* **2018**, *24*, 9377−9384.

https://doi.org/10.1021/acs.inorgchem.3c03532
Inorg. Chem. 2024, 63, 1589−1606

(32) Shafikov, M. Z.; Kozhevnikov, D. N.; Bodensteiner, M.; Brandl, F.; Czerwieniec, R. Modulation of Intersystem Crossing Rate by Minor Ligand Modifications in Cyclometalated Platinum(II) Complexes. *Inorg. Chem.* **2016**, *55*, 7457−7466.
(33) (a) Kui, S. C. F.; Hung, F.-F.; Lai, S.-L.; Yuen, M.-Y.; Kwok, C.-C.; Low, K.-H.; Chui, S. S.-Y.; Che, C.-M. Luminescent Organoplatinum(II) Complexes with Functionalized Cyclometalated C^N^C Ligands: Structures, Photophysical Properties, and Material Applications. *Chem.—Eur. J.* **2012**, *18*, 96−109. (b) Wan, S.; Lu, W. Reversible Photoactivated Phosphorescence of Gold(I) Arylethynyl Complexes in Aerated DMSO Solutions and Gels. *Angew. Chem., Int. Ed.* **2017**, *56*, 1784−1788.
(34) Sagadevan, A.; Hwang, K. C.; Su, M.-D. Singlet oxygen-mediated selective C−H bond hydroperoxidation of ethereal hydrocarbons. *Nat. Commun.* **2017**, *8*, 1812.
(35) (a) Flors, C.; Nonell, S. Light and Singlet Oxygen in Plant Defense Against Pathogens: Phototoxic Phenalenone Phytoalexins. *Acc. Chem. Res.* **2006**, *39*, 293−300. (b) Silva, E. F. F.; Schaberle, F. A.; Monteiro, C. J. P.; Dąbrowski, J. M.; Arnaut, L. G. The challenging combination of intense fluorescence and high singlet oxygen quantum yield in photostable chlorins — a contribution to theranostics. *Photochem. Photobiol. Sci.* **2013**, *12*, 1187−1192. (c) Trivella, A. S.; Monadjemi, S.; Worrall, D. R.; Kirkpatrick, I.; Arzoumanian, E.; Richard, C. Perinaphthenone phototransformation in a model of leaf epicuticular waxes. *J. Photochem. Photobiol. B Biol.* **2014**, *130*, 93−101. (d) Godard, J.; Brégier, F.; Arnoux, P.; Myrzakhmetov, B.; Champavier, Y.; Frochot, C.; Sol, V. New Phenalenone Derivatives: Synthesis and Evaluation of Their Singlet Oxygen Quantum Yield. *ACS Omega* **2020**, *5*, 28264−28272. (e) Kaye, E. G.; Kailass, K.; Sadovski, O.; Beharry, A. A. A Green-Absorbing, Red-Fluorescent Phenalenone-Based Photosensitizer as a Theranostic Agent for Photodynamic Therapy. *ACS Med. Chem. Lett.* **2021**, *12*, 1295−1301. (f) Payne, D. T.; Hynek, J.; Labuta, J.; Hill, J. P. Nonionic omnisoluble photosensitizer reference material for the estimation of singlet oxygen quantum yield. *Phys. Chem. Chem. Phys.* **2022**, *24*, 6146−6154. (g) Gómez de Segura, D.; Giménez, N.; Rincón-Montón, D.; Moreno, M. T.; Pichel, J. G.; López, I. P.; Lalinde, E. A new family of luminescent $[Pt(pbt)_2\ (C_6F_5)L]^{n+}$ (n = 1, 0) complexes: synthesis, optical and cytotoxic studies. *Dalton Trans.* **2023**, *52*, 12390−12403.
(36) Muraveiskaya, G. S.; Kuklna, G. A.; Orlova, V. S.; Evstaf'eva, O. N.; Porai-Koshits, M. A. Pt(III) sulfates with metal-metal bond. Synthesis and structure. *Dokl. Akad. Nauk SSSR* **1976**, *226*, 596.
(37) (a) Matsumoto, K.; Ochiai, M. Organometallic chemistry of platinum-blue derived platinum^{III} dinuclear complexes. *Coord. Chem. Rev.* **2002**, *231*, 229−238. (b) Umakoshi, K.; Sasaki, Y. *Adv. Inorg. Chem.*; Sykes, A. G., Ed.; Academic Press, 1993; Vol. *40*, p 187. (c) Matsumoto, K.; Arai, S.; Ochiai, M.; Chen, W.; Nakata, A.; Nakai, H.; Kinoshita, S. Synthesis of the Pivalamidate-Bridged Pentanuclear Platinum(II,III) Linear Complexes with Pt···Pt Interactions. *Inorg. Chem.* **2005**, *44*, 8552−8560. (d) Santoro, A.; Wegrzyn, M.; Whitwood, A. C.; Donnio, B.; Bruce, D. W. Oxidation of Organoplatinum(II) by Coordinated Dimethylsulfoxide: Metal−Metal Bonded, Dinuclear, Liquid-Crystalline Complexes of Platinum(III). *J. Am. Chem. Soc.* **2010**, *132*, 10689−10691. (e) Whitfield, S. R.; Sanford, M. S. Reactions of Platinum(II) Complexes with Chloride-Based Oxidants: Routes to Pt(III) and Pt(IV) Products. *Organometallics* **2008**, *27*, 1683−1689. (f) Anger, E.; Rudolph, M.; Shen, C.; Vanthuyne, N.; Toupet, L.; Roussel, C.; Autschbach, J.; Crassous, J.; Réau, R. From Hetero- to Homochiral Bis(metallahelicene)s Based on a Pt^{III}−Pt^{III} Bonded Scaffold: Isomerization, Structure, and Chiroptical Properties. *J. Am. Chem. Soc.* **2011**, *133*, 3800−3803.
(38) Bandoli, G.; Caputo, P. A.; Intini, F. P.; Sivo, M. F.; Natile, G. Synthesis and X-ray Structural Characterization of Two Unbridged Diplatinum(III) Compounds: cis- and trans-Bis[bis(1-imino-1-methoxyethane)trichloroplatinum(III)]. Transient Species in the Oxidation of Platinum(II) to Platinum(IV). *J. Am. Chem. Soc.* **1997**, *119*, 10370−10376.
(39) Soto, M. A.; Carta, V.; Andrews, R. J.; Chaudhry, M. T.; MacLachlan, M. J. Structural Elucidation of Selective Solvatochromism in a Responsive-at-Metal Cyclometalated Platinum(II) Complex. *Angew. Chem., Int. Ed.* **2020**, *59*, 10348−10352.
(40) Ochiai, M.; Fukui, K.; Iwatsuki, S.; Ishihara, K.; Matsumoto, K. Synthesis of Aryl-Platinum Dinuclear Complexes via ortho C−H Bond Activation of Phenol and Transmetalation of Arylboronic Acid. *Organometallics* **2005**, *24*, 5528−5536.
(41) Stiegman, A. E.; Miskowski, V. M.; Gray, H. B. Metal-metal excited-state emission from binuclear platinum (III) complexes. *J. Am. Chem. Soc.* **1986**, *108*, 2781−2782.
(42) (a) Aoki, R.; Kobayashi, A.; Chang, H. C.; Kato, M. Structures and Luminescence Properties of Cyclometalated Dinuclear Platinum-(II) Complexes Bridged by Pyridinethiolate Ions. *Bull. Chem. Soc. Jpn.* **2011**, *84*, 218−225. (b) Chaaban, M.; Chi, Y.-C.; Worku, M.; Zhou, C.; Lin, H.; Lee, S.; Ben-Akacha, A.; Lin, X.; Huang, C.; Ma, B. Thiazol-2-thiolate-Bridged Binuclear Platinum(II) Complexes with High Photoluminescence Quantum Efficiencies of up to Near Unity. *Inorg. Chem.* **2020**, *59*, 13109−13116.
(43) Wang, Z.; Jiang, L.; Liu, Z.-P.; Gan, C. R. R.; Liu, Z.; Zhang, X.-H.; Zhao, J.; Hor, T. S. A. Facile formation and redox of benzoxazole-2-thiolate-bridged dinuclear Pt(II/III) complexes. *Dalton Trans.* **2012**, *41*, 12568.
(44) (a) Melchiorre, P. Introduction: Photochemical Catalytic Processes. *Chem. Rev.* **2022**, *122*, 1483−1484. (b) Marzo, L.; Pagire, S. K.; Reiser, O.; König, B. Visible-Light Photocatalysis: Does It Make a Difference in Organic Synthesis? *Angew. Chem., Int. Ed.* **2018**, *57*, 10034−10072. (c) Lang, X.; Chen, X.; Zhao, J. Heterogeneous visible light photocatalysis for selective organic transformations. *Chem. Soc. Rev.* **2014**, *43*, 473−486. (d) Prier, C. K.; Rankic, D. A.; MacMillan, D. W. C. Visible Light Photoredox Catalysis with Transition Metal Complexes: Applications in Organic Synthesis. *Chem. Rev.* **2013**, *113*, 5322−5363.
(45) (a) Strieth-Kalthoff, F.; James, M. J.; Teders, M.; Pitzer, L.; Glorius, F. Energy transfer catalysis mediated by visible light: principles, applications, directions. *Chem. Soc. Rev.* **2018**, *47*, 7190−7202. (b) Schmid, L.; Glaser, F.; Schaer, R.; Wenger, O. S. High Triplet Energy Iridium(III) Isocyanoborato Complex for Photochemical Upconversion, Photoredox and Energy Transfer Catalysis. *J. Am. Chem. Soc.* **2022**, *144*, 963−976.
(46) (a) Ahmed, S.; Kumar, A.; Mukherjee, P. S. A benzothiadiazole-based Pt(II) coordination polymer as an efficient heterogeneous photocatalyst for visible-light-driven aerobic oxidative coupling of amines. *Chem. Commun.* **2023**, *59*, 3229−3232. (b) Wu, W.; Yang, P.; Ma, L.; Lalevée, J.; Zhao, J. Visible-Light Harvesting Pt^{II} Complexes as Singlet Oxygen Photosensitizers for Photooxidation of 1,5-Dihydroxynaphthalene. *Eur. J. Inorg. Chem.* **2013**, *2013*, 228−231. (c) Jin, J.; Shin, H.-W.; Park, J. H.; Park, J. H.; Kim, E.; Ahn, T. K.; Ryu, D. H.; Son, S. U. Iridium Complexes Containing Bis(imidazoline thione) and Bis(imidazoline selone) Ligands for Visible-Light-Induced Oxidative Coupling of Benzylamines to Imines. *Organometallics* **2013**, *32*, 3954−3959. (d) Echevarría, I.; Vaquero, M.; Manzano, B. R.; Jalón, F. A.; Quesada, R.; Espino, G. Photocatalytic Aerobic Dehydrogenation of N-Heterocycles with Ir(III) Photosensitizers Bearing the 2(2′-Pyridyl)-benzimidazole Scaffold. *Inorg. Chem.* **2022**, *61*, 6193−6208.
(47) (a) Vaquero, M.; Ruiz-Riaguas, A.; Martínez-Alonso, M.; Jalón, F. A.; Manzano, B. R.; Rodríguez, A. M.; García-Herbosa, G.; Carbayo, A.; García, B.; Espino, G. Selective Photooxidation of Sulfides Catalyzed by Bis-cyclometalated Ir^{III} Photosensitizers Bearing 2,2′-Dipyridylamine-Based Ligands. *Chem.—Eur. J.* **2018**, *24*, 10662−10671. (b) Chao, D.; Zhao, M. Robust Cooperative Photo-oxidation of Sulfides without Sacrificial Reagent under Air Using a Dinuclear Ru^{II}−Cu^{II} Assembly. *ChemSusChem* **2017**, *10*, 3358−3362. (c) Zen, J.-M.; Liou, S.-L.; Kumar, A. S.; Hsia, M.-S. An Efficient and Selective Photocatalytic System for the Oxidation of Sulfides to Sulfoxides. *Angew. Chem., Int. Ed.* **2003**, *42*, 577−579. (d) Li, J.; An, Z.; Sun, J.; Tan, C.; Gao, D.; Tan, Y.; Jiang, Y. Highly Selective Oxidation of Organic Sulfides by a Conjugated Polymer as the Photosensitizer for Singlet Oxygen Generation. *ACS Appl. Mater. Interfaces* **2020**, *12*, 35475−35481. (e) Liang, X.; Guo, Z.; Wei, H.; Liu, X.; Lv, H.; Xing, H. Selective photooxidation of sulfides mediated by singlet oxygen using

https://doi.org/10.1021/acs.inorgchem.3c03532
Inorg. Chem. 2024, 63, 1589−1606

visible-light-responsive coordination polymers. *Chem. Commun.* **2018**, *54*, 13002−13005.
(48) (a) Rubino, S.; Busà, R.; Attanzio, A.; Alduina, R.; Di Stefano, V.; Girasolo, M. A.; Orecchio, S.; Tesoriere, L. Synthesis, properties, antitumor and antibacterial activity of new Pt(II) and Pd(II) complexes with 2,2′-dithiobis(benzothiazole) ligand. *Bioorg. Med. Chem.* **2017**, *25*, 2378−2386. (b) Ye, C.; Zhang, Y.; Ding, A.; Hu, Y.; Guo, H. Visible light sensitizer-catalyzed highly selective photo oxidation from thioethers into sulfoxides under aerobic condition. *Sci. Rep.* **2018**, *8*, 2205.
(49) (a) Bonesi, S. M.; Manet, I.; Freccero, M.; Fagnoni, M.; Albini, A. Photosensitized Oxidation of Sulfides: Discriminating between the Singlet-Oxygen Mechanism and Electron Transfer Involving Superoxide Anion or Molecular Oxygen. *Chem.—Eur. J.* **2006**, *12*, 4844−4857. (b) Baciocchi, E.; Giacco, T. D.; Elisei, F.; Gerini, M. F.; Guerra, M.; Lapi, A.; Liberali, P. Electron Transfer and Singlet Oxygen Mechanisms in the Photooxygenation of Dibutyl Sulfide and Thioanisole in MeCN Sensitized by N-Methylquinolinium Tetrafluoborate and 9,10-Dicyanoanthracene. The Probable Involvement of a Thiadioxirane Intermediate in Electron Transfer Photooxygenations. *J. Am. Chem. Soc.* **2003**, *125*, 16444−16454.

https://doi.org/10.1021/acs.inorgchem.3c03532
Inorg. Chem. 2024, 63, 1589−1606